

October 10th, 2015

Editor for Atmospheric Chemistry and Physics

Dear Editor Dr. Pusede,

Thank you for your support of this study. We are re-submitting the manuscript entitled “Distinguishing the drivers of trends in land carbon fluxes and plant volatile emissions over the past three decades” to *Atmospheric Chemistry and Physics*.

In response to your first concern about the uniqueness of YIBs model, we added the following statement in the Introduction section:

“The YIBs model provides a unique tool to identify drivers of decadal trends in carbon fluxes and BVOC emissions because of the distinct treatments of plant phenology and BVOC emissions. Many state-of-art vegetation models suffer from poor representations of phenology, which may lead to large biases in the simulated carbon fluxes (Richardson et al., 2012). The optimized phenology in YIBs is based on assessment of 13 existing models (9 for spring and 4 for autumn), and has been validated against both ground-based records and multiple satellite retrievals (Yue et al., 2015). In addition, YIBs incorporates two independent isoprene emission schemes within the exact same host model framework (Unger et al., 2013; Zheng et al., 2015) (i) a photosynthesis-dependent isoprene emission scheme (Niinemets et al., 1999), and (ii) the Model of Emissions of Gases and Aerosols from Nature (MEGAN) isoprene scheme (Guenther et al., 2012) that is widely used in chemistry-transport modeling. Therefore, the YIBs model allows us to investigate modeling uncertainties due to the differences in the BVOC emission algorithms themselves.”

For your second concern about the brief explanation of the purpose for model comparison, we have added the following statement in the beginning of section 4.2:

“We assess the YIBs simulations within the context of other models and/or previous multi-model studies to evaluate the robustness of the predicted trends in land carbon fluxes and BVOC emissions.”

A mark-up version of manuscript is attached.

Thanks for your consideration of our submission.

Sincerely,

Xu Yue
School of Forestry and Environmental Studies
Yale University
New Haven, CT, 06511, USA
E-mail: xuyueseas@gmail.com

1 **Distinguishing the drivers of trends in land carbon fluxes and plant volatile**
2 **emissions over the past three decades**

3
4 X. Yue ¹, N. Unger ¹, Y. Zheng ²

5
6 ¹ School of Forestry and Environment Studies, Yale University, New Haven, Connecticut
7 06511, USA
8 ² Department of Geology and Geophysics, Yale University, New Haven, Connecticut
9 06511, USA

10
11
12
13 *Correspondence to:* X. Yue (xuyueseas@gmail.com)
14
15

Abstract

16
17
18 The terrestrial biosphere has experienced dramatic changes in recent decades. Estimates
19 of historical trends in land carbon fluxes remain uncertain because long-term
20 observations are limited on the global scale. Here, we use the Yale Interactive terrestrial
21 Biosphere (YIBs) model to estimate decadal trends in land carbon fluxes and emissions
22 of biogenic volatile organic compounds (BVOCs) and to identify the key drivers for these
23 changes during 1982-2011. Driven with hourly meteorology from WFDEI (WATCH
24 Forcing Data methodology applied to ERA-Interim data), the model simulates an
25 increasing trend of 297 Tg C a^{-2} in gross primary productivity (GPP) and 185 Tg C a^{-2} in
26 the net primary productivity (NPP). CO_2 fertilization is the main driver for the flux
27 changes in forest ecosystems, while meteorology dominates the changes in grasslands
28 and shrublands. Warming boosts summer GPP and NPP at high latitudes, while drought
29 dampens carbon uptake in tropical regions. North of 30°N , increasing temperatures
30 induce a substantial extension of 0.22 day a^{-1} for the growing season; however, this
31 phenological change alone does not promote regional carbon uptake and BVOC
32 emissions. Nevertheless, increases of LAI at peak season accounts for $\sim 25\%$ of the trends
33 in GPP and isoprene emissions at the northern lands. The net land sink shows statistically
34 insignificant increases of only 3 Tg C a^{-2} globally because of simultaneous increases in
35 soil respiration. Global BVOC emissions are calculated using two schemes. With the
36 photosynthesis-dependent scheme, the model predicts increases of 0.4 Tg C a^{-2} in
37 isoprene emissions, which are mainly attributed to warming trends because CO_2
38 fertilization and inhibition effects offset each other. Using the MEGAN (Model of
39 Emissions of Gases and Aerosols from Nature) scheme, the YIBs model simulates global
40 reductions of 1.1 Tg C a^{-2} in isoprene and 0.04 Tg C a^{-2} in monoterpene emissions in
41 response to the CO_2 inhibition effects. Land use change shows limited impacts on global
42 carbon fluxes and BVOC emissions, but there are regional contrasting impacts over
43 Europe (afforestation) and China (deforestation).
44

45 **1 Introduction**

46

47 The terrestrial biosphere interacts with the atmosphere through photosynthesis and
48 biogenic volatile organic compound (BVOC) emissions. Annually, terrestrial ecosystems
49 assimilate ~120 petagrams of carbon (Pg C) from the atmosphere (Beer et al., 2010),
50 most of which reenters atmosphere through respiration and decomposition, resulting in a
51 net global land carbon sink of $2.6 \pm 0.7 \text{ Pg C a}^{-1}$ (Le Quere et al., 2009; Sitch et al.,
52 2015). Global BVOC emissions are estimated to be about 1 Pg C per year (Carslaw et al.,
53 2010). These emissions are important precursors of atmospheric oxidants and aerosols,
54 both of which affect surface air quality and exert additional regional and global chemical
55 climate forcings (Scott et al., 2014; Unger, 2014). Observations and simulations have
56 shown significant changes in terrestrial carbon assimilation and BVOC emissions in the
57 past 2-3 decades (Lathiere et al., 2006; Sarmiento et al., 2010; Sindelarova et al., 2014;
58 Sitch et al., 2015). Understanding drivers of these trends is important for the projections
59 of future carbon fluxes, water cycle, air quality, and climatic responses.

60

61 Trends in land carbon assimilation and BVOC emissions are related to the changes in
62 atmospheric CO₂, meteorology, and human land use land cover change perturbations.
63 Elevated CO₂ promotes plant photosynthesis (Ainsworth and Long, 2005) but can
64 directly inhibit isoprene productions (Arneth et al., 2007). Warming accelerates both
65 carbon uptake and BVOC emissions when temperature is not above the thermal optimum
66 (25-30 °C for photosynthesis and 35-40 °C for isoprene emission) for ecosystems that are
67 not water-stressed (Farquhar et al., 1980; Guenther et al., 1993; Piao et al., 2013).
68 Additional warming above thermal optimum may decrease photosynthesis but still
69 promote respiration, reducing net carbon uptake by plants (Liang et al., 2013). Increased
70 temperatures also indirectly influence carbon exchange and BVOC emissions through the
71 extension of growing season (Piao et al., 2007). Drought decreases gross primary
72 productivity (GPP) and net primary productivity (NPP) (Zhao and Running, 2010), but
73 may temporally enhance isoprene emissions (Monson et al., 2007). Land use change
74 affects the regional carbon budget and BVOC emissions through either additional

75 emissions or land cover changes due to deforestation, forest management, and
76 agricultural activities (Lathiere et al., 2006; Houghton, 2010).

77

78 Estimates of recent decadal global trends in the land carbon budget and BVOC emissions
79 are limited and uncertain due to the lack of observations. The earliest site-level
80 measurements of land carbon fluxes were set up in the 1990s (Wofsy et al., 1993). The
81 flux tower data sets provide long-term records of regional carbon exchange with high
82 precision but low spatial representation. In contrast, satellite products, such as GPP and
83 NPP retrievals from the Moderate Resolution Imaging Spectroradiometer (MODIS)
84 (Zhao et al., 2005) and isoprene emissions based on tropospheric formaldehyde columns
85 from the Global Ozone Monitoring Experiment (Palmer et al., 2006), improve the spatial
86 coverage but usually are available for only a relatively short time period (months to
87 several years) and suffer from systematic biases when compared with ground
88 measurements (e.g., Heinsch et al., 2006; Marais et al., 2012). Terrestrial biosphere
89 models, evaluated with both site-level and satellite-based observations, are useful tools to
90 estimate trends and attribute drivers of changes in land carbon fluxes and BVOC
91 emissions (e.g., Mao et al., 2013; Stavrakou et al., 2014; Sitch et al., 2015).

92

93 In this study, we use the Yale Interactive Terrestrial Biosphere Model (YIBs, Yue and
94 Unger, 2015) driven with long-term reanalysis meteorology to study the global trends of
95 land carbon fluxes and BVOC emissions over the past three decades. The YIBs model is
96 a process-based vegetation model that simulates complete land carbon cycle, including
97 photosynthesis, plant/soil respiration, carbon allocation, and tree growth. Simulated
98 carbon fluxes has been fully validated with carbon fluxes from 145 flux tower sites and
99 multiple satellite products (Yue and Unger, 2015). The YIBs model provides a unique
100 tool to identify drivers of decadal trends in carbon fluxes and BVOC emissions because
101 of the distinct treatments of plant phenology and BVOC emissions. Many state-of-art
102 vegetation models suffer from poor representations of phenology, which may lead to
103 large biases in the simulated carbon fluxes (Richardson et al., 2012). The optimized
104 phenology in YIBs is based on assessment of 13 existing models (9 for spring and 4 for
105 autumn), and has been validated against both ground-based records and multiple satellite

Xu Yue 10/10/15 6:48 PM

Deleted: including complete land carbon cycle (photosynthesis, plant/soil respiration, carbon allocation, and tree growth), plant phenology (Yue et al., 2015), and two independent schemes of BVOC emissions (Zheng et al., 2015).

112 retrievals (Yue et al., 2015). In addition, YIBs incorporates two independent isoprene
113 emission schemes within the exact same host model framework (Unger et al., 2013;
114 Zheng et al., 2015) (i) a photosynthesis-dependent isoprene emission scheme (Niinemets
115 et al., 1999), and (ii) the Model of Emissions of Gases and Aerosols from Nature
116 (MEGAN) isoprene scheme (Guenther et al., 2012) that is widely used in chemistry-
117 transport modeling. Therefore, the YIBs model allows us to investigate modeling
118 uncertainties due to the differences in the BVOC emission algorithms themselves. The
119 major goals of this study are to identify: (1) the dominant drivers of the 30-year trends in
120 carbon fluxes and BVOC emissions from elevated CO₂, changes in meteorology
121 (temperature, radiation, and soil moisture), and human land use change; (2) the feedback
122 of biosphere, including changes in phenology and leaf area index (LAI), to the trends of
123 land carbon uptakes and BVOC emissions; and (3) the discrepancies in BVOC trends due
124 to application of different isoprene emission schemes.

125

126

127 **2 Data and methods**

128

129 **2.1 Observations and benchmark products**

130

131 We use long-term global measurements of LAI, GPP, and NPP to validate the simulated
132 trends. The LAI dataset for 1982-2011 is retrieved based on the Normalized Difference
133 Vegetation Index (NDVI) from Global Inventory Modeling and Mapping Studies
134 (GIMMS) with 1/12 degree resolution and a 15-day interval (Zhu et al., 2013). We also
135 use LAI data for 2000-2011 from the MODIS (<http://modis.gsfc.nasa.gov/>). GPP
136 benchmark products of 1982-2011 are upscaled from the FLUXNET eddy covariance
137 measurements using an ensemble of regression trees (Jung et al., 2009). As a comparison,
138 we also use the GPP and NPP datasets for 2000-2011 from the MODIS, which have been
139 developed based on remote sensing of biome parameters and assimilated meteorology
140 (Zhao et al., 2005). All the datasets are interpolated to the monthly interval at the 1°×1°
141 off-line YIBs model resolution.

142

143 2.2 Model

144

145 The YIBs model is a process-based terrestrial vegetation model that simulates the land
146 carbon budget and dynamic tree growth (Yue and Unger, 2015). The model adapts
147 routines from the mature TRIFFID (Cox, 2001) and CASA (Schaefer et al., 2008) models
148 with special updates in the parameterizations of ozone vegetation damage (Yue and
149 Unger, 2014), plant phenology (Yue et al., 2015), and the photosynthesis-dependent
150 isoprene emission (Unger et al., 2013). The model simulates carbon uptake for 9 plant
151 functional types (PFTs) including tundra, C3/C4 grass, shrubland, deciduous broadleaf
152 forest (DBF), ENF evergreen needleleaf forest (ENF), evergreen broadleaf forest (EBF),
153 and C3/C4 cropland. The vegetation biophysics calculates leaf-level photosynthesis using
154 the well-established Farquhar scheme (Farquhar et al., 1980; von Caemmerer and
155 Farquhar, 1981) and the stomatal conductance model of Ball and Berry (Collatz et al.,
156 1991). The canopy radiative transfer scheme computes direct and diffuse
157 photosynthetically active radiation (PAR) for sunlit and shaded regions for an adaptive
158 number of layers. The leaf photosynthesis is then integrated over all canopy layers to
159 generate the GPP.

160

161 Part of the assimilated carbon is used for maintenance and growth respiration, and the
162 rest is allocated among different pools for plant development. The model calculates
163 phenology for deciduous forests using cumulative temperature summation with additional
164 constraints from chilling and photoperiod (Yue et al., 2015). The phenology of shrubland
165 and grassland is jointly determined by the temperature- and drought-dependent metrics.
166 The LAI is then updated daily based on phenology and the net carbon assimilation. The
167 soil respiration scheme considers carbon flows among 12 biogeochemical pools,
168 including 3 live pools and 9 dead pools. The land carbon source or sink is calculated as
169 the difference between the net carbon assimilation and soil respiration.

170

171 The YIBs model incorporates two independent leaf-level isoprene emission schemes
172 embedded within the exact same host model framework (Zheng et al., 2015). The
173 photosynthesis-based (PS_BVOC) isoprene scheme calculates emissions based on the

174 electron transport-limited photosynthesis rate, canopy temperature, and intercellular CO₂
175 concentrations (Niinemets et al., 1999; Arneth et al., 2007; Unger et al., 2013). The
176 MEGAN scheme applies commonly used leaf-level empirical functions of light and
177 canopy temperature (Guenther et al., 1993). Both schemes implement CO₂ inhibition
178 effects on BVOC emissions parameterized as a reciprocal empirical function of
179 intercellular [CO₂] following the observations from Possell et al. (2005). For
180 monoterpene emissions, the YIBs model applies the same temperature-dependent scheme
181 as Lathiere et al. (2006) but with CO₂-inhibition effects. The leaf-level BVOC emissions
182 are integrated over the multiple canopy layers following the same approach as GPP to
183 obtain the total canopy-level emissions.

184

185 YIBs can be used in three different configurations with increasing complexity: (1) off-
186 line local site level, which is driven with hourly measurements of CO₂ concentrations and
187 meteorology at flux tower sites; (2) off-line global forced with spatially uniform but
188 annually updated CO₂ concentrations and hourly gridded reanalysis meteorology; (3) on-
189 line coupled to the NASA ModelE2 driven with simulated meteorology by the GCM
190 every half hour. At the site level, YIBs simulates reasonable seasonality (correlation
191 coefficient $R > 0.8$) of GPP at 121 out of 145 flux-tower sites with biases in magnitude
192 ranging from -19 to 7 % depending on PFTs. On the global scale, the offline model
193 simulates an annual GPP of 125 ± 3 Pg C and net ecosystem exchange (NEE) of $-2.5 \pm$
194 0.7 Pg C for 1982-2011, with seasonality and spatial distribution consistent with both
195 satellite observations and benchmark synthesis products (Yue and Unger, 2015).
196 However, the model does not include a fully coupled carbon-nitrogen cycle, which may
197 overestimate CO₂ fertilization effects. In addition, phenology of evergreen trees is set to
198 constant value of 1, leading to underestimation of phenological feedbacks to flux trends.
199 In this study, we use the (2) off-line global version of the model, which is driven with
200 global meteorology reanalysis data and observed CO₂ concentrations.

201

202 2.3 Simulations

203

Xu Yue 10/10/15 6:48 PM

Deleted: (Arneth et al., 2007; Unger et al., 2013)

Xu Yue 10/10/15 6:48 PM

Deleted: . The Model of Emissions of Gases and Aerosols from Nature (MEGAN) scheme applies commonly used leaf-level empirical functions of light and canopy temperature.

210 We apply observed historical atmospheric CO₂ concentrations from the fifth assessment
211 report (AR5) of the Intergovernmental Panel on Climate Change (IPCC) (Meinshausen et
212 al., 2011). We apply an annually-varying historical transient land cover dataset (Oleson et
213 al., 2013), which is developed based on a combination of remote sensing data from both
214 MODIS (Hansen et al., 2003) and the Advanced Very High Resolution Radiometer
215 (AVHRR) (Defries et al., 2000), and with land use change from Hurtt et al. (2011). We
216 use hourly meteorological variables for 1980-2011 from the WATCH Forcing Data
217 methodology applied to ERA-Interim data (WFDEI, Weedon et al., 2014). The WFDEI
218 reanalysis is an update of the WATCH Forcing Data (WFD), which is developed based
219 on the European Centre for Medium-range Weather Forecasts (ECMWF) ERA-40
220 reanalysis (Uppala et al., 2005). Meteorological variables applied include surface air
221 temperature, specific humidity, wind speed, surface pressure, total PAR, and soil
222 temperature and wetness. All of the forcing data are interpolated to the 1°×1° model
223 resolution at the hourly interval.

224

225 We perform 10 sensitivity simulations to distinguish driving factors for the changes in
226 land carbon fluxes and BVOC emissions in the past 3 decades (Table 1). The control
227 simulation (CO2_MET_LUC) uses interannually-varying meteorology, [CO₂], and land
228 cover for 1980-2011. The CO2_MET run is the same as the control simulation but
229 prescribes land cover at the year 1980. Three single-factor runs prescribe most boundary
230 conditions at the year 1980 but allow the interannual variations of [CO₂] (CO2_ONLY),
231 land cover (LUC_ONLY), and meteorology (MET_ONLY) respectively. Results from
232 these runs are compared with that of control simulation to determine the dominant drivers
233 of simulated trends. To understand the impact of individual meteorological variables,
234 three additional runs are performed with fixed (or recycled) [CO₂], land cover, and all
235 meteorology at year 1980 but one field varying for 1980-2011 each time, including
236 temperature (TEMP_ONLY), PAR (PAR_ONLY), and soil wetness (SOILW_ONLY).
237 Finally, two runs are performed to examine feedback of biospheric changes. LAI_ONLY
238 prescribes all boundary conditions at the starting year 1980 but implements the year-to-
239 year LAI simulated by the control run. PHEN_ONLY also prescribes all forcings at the
240 starting year except for the year-to-year phenology from control simulation. All

241 simulations are initialized following the same spin up process (Yue and Unger, 2015) and
242 are integrated for 1980-2011.

243

244

245 **3 Results**

246

247 **3.1 Drivers of trends in LAI**

248

249 Observations show an increasing trend of LAI on most of vegetated continents, especially
250 in Europe, northern and eastern Asia, central Africa, and southeastern U.S. in the past 3
251 decades (Fig. 1a). The simulation with year-to-year [CO₂], land cover, and meteorology
252 reproduces the magnitude of trend in Europe and the sign of trend in northern Asia,
253 eastern U.S., central Asia, and Australia (Fig. 1b). The model predicts negative changes
254 in central Africa, western U.S., eastern Asia, and the east of South America, which are
255 inconsistent with satellite observations. These negative trends are mainly contributed by
256 the changes in meteorology (Fig. 1e), except for that in East Asia where land cover
257 changes due to human activities result in the decline of LAI (Fig. 1f). Without the land
258 use perturbation, the negative LAI trend in East Asia is weakened and the prediction is
259 closer to observations (Fig. 1c). For the individual drivers, CO₂ fertilization leads to
260 widespread increases in LAI (Fig. 1d), meteorology causes dipole changes on most
261 continents (Fig. 1e), and land use change generally results in negative trends (Fig. 1f).
262 Regionally, simulation CO₂_MET_LUC shows a positive trend of 0.0035 m² m⁻² a⁻¹ in
263 Europe (Table 2), close to the observed value of 0.0049 m² m⁻² a⁻¹ (Fig. 1a). In other
264 areas, simulated LAI trends are either underestimated (by 87% in Amazon, 78% in North
265 America, and 48% in Central Africa) or opposite in sign (East Asia and Indonesia)
266 compared to observations. Such inconsistencies indicate the limit of model simulations,
267 but may also in part result from the uncertainties in the satellite measurements (see
268 section 4.1).

269

270 **3.2 Drivers of trends in land carbon fluxes**

271

272 Predicted GPP and NPP trends show similar spatial pattern as that of LAI (Figs. 2a and
273 2c). However, regional trends are all positive in the main continents and on the global
274 scale (Tables 2 and 3). Tropical areas are experiencing maximum changes, especially in
275 Central Africa (GPP by 83.3 Tg C a⁻² and NPP by 51.7 Tg C a⁻²) and the Amazon (52.7
276 and 27.1 Tg C a⁻²). In the Northern Hemisphere (NH), changes are significant in Europe
277 (53.4 and 33.2 Tg C a⁻²), East Asia (42.4 and 27.2 Tg C a⁻²), and North America (13.6
278 and 9.7 Tg C a⁻²). 30-year historical observations of GPP and NPP are not available.
279 Therefore, we compare YIBs predictions with MODIS land carbon fluxes over the more
280 recent period of 2000-2011 (Fig. 3). Different from the 30-year trend, land carbon fluxes
281 over the recent decade show negative trends in southeastern U.S., southern Africa,
282 eastern Australia, and central and northern Asia (Figs. 3a and 3c). Most of these changes
283 are consistent with the MODIS observations (except for the U.S., Figs. 3b and 3d) and
284 are attributed to the drought tendency in the past decade (Zhao and Running, 2010).

285

286 For the 30-year trend, both CO₂ and meteorology are playing important roles (Figs. 2b
287 and 2d). CO₂ fertilization dominates the GPP and NPP trends of tropical forests in the
288 Amazon, central Africa, and Indonesia, and ENF and DBF in boreal North America,
289 eastern Europe, and central and northern Asia. Land use change plays a limited role in
290 land carbon cycle flux trends over the past 3 decades, except for some areas in northern
291 Africa. Meteorological forcing drives changes in land carbon fluxes for tundra in
292 subarctic regions, C3 grasslands in the central U.S. and southern Africa, C4 grasslands in
293 central Africa and the east of South America, and shrublands in Australia and southern
294 Asia. Soil wetness plays the dominant role in the tropical and subtropical areas (Fig. 4b).
295 The drought tendency in the western U.S., central Africa, and the east of South America
296 (Fig. S1d) results in the regional decline of land carbon fluxes (Fig. 4a). In contrast, the
297 increasing wetness in the northern Amazon and southern Africa leads to the enhancement
298 of regional GPP. Warming is the main cause for the GPP trends over the subarctic areas
299 (Fig. 4b). Contribution of PAR is limited, except for some areas in the eastern Europe.

300

301 The simulated net ecosystem productivity (NEP) shows weaker trends compared with
302 GPP and NPP (Fig. 2e), because NEP is offset by the significant trends in heterotrophic

303 respiration (Rh) (Table 2). Regionally, the YIBs model predicts enhanced net land carbon
304 uptake in boreal North America, northern Asia, and southern Africa but reduced NEP in
305 the central U.S., the Amazon, central Africa, eastern Europe, and East Asia. The
306 simulated global NEP trends (Fig. 5d) are in broad agreement with the comprehensive
307 bottom-up estimates by Pan et al. (2011), who found slightly decreasing net carbon
308 uptake by global established forests (without human perturbations in the tropics but with
309 afforestation in subtropical areas) in 2000-2007 relative to that in 1990-1999. Attribution
310 analysis shows that the NEP trends are mainly driven by the changes in meteorological
311 forcings (Fig. 2f), because CO₂ fertilization enhances both NPP and Rh with similar
312 magnitude (Fig. 5).

313

314 On the global scale, GPP, NPP, and Rh increase respectively by 298, 185, and 181 Tg C
315 a⁻² in the past 3 decades (Table 3). The long-term trends of carbon fluxes are mainly
316 driven by CO₂ fertilization, while the interannual variability is related to meteorological
317 forcings (Fig. 5). Warming alone decreases GPP especially in tropical forests (not shown)
318 but increases autotrophic respiration (Ra), leading to global reductions of 56 Tg C a⁻² in
319 NPP and 10 Tg C a⁻² in NEP (Table 3). Drought alone strongly decreases GPP, especially
320 for tropical grassland and shrubland (Fig. 4), leading to reductions of 51 Tg C a⁻² in NPP
321 and 13 Tg C a⁻² in NEP. Trends in PAR do not affect GPP and NPP, but may decrease
322 NEP by 23 Tg C a⁻² because soil respiration is slowly increasing to reach the equilibrium.
323 Land use change has very limited impacts on the trends of carbon fluxes, though it
324 induces relatively large reductions in NEP (Table 3).

325

326 **3.3 Drivers of trends in BVOC emissions**

327

328 Simulated isoprene emission trends are sensitive to the choice of modeling scheme. With
329 the PS_BVOC scheme, global isoprene emissions increase by 0.4 Tg C a⁻² during 1982-
330 2011. Large enhancements are predicted in central Africa (0.25 Tg C a⁻²) and Europe
331 (0.16 Tg C a⁻²), while moderate reductions are found in the western U.S., eastern South
332 America, and East Asia (Fig. 6a). Drought accounts for the decline of isoprene emissions
333 in the U.S. and South America, but land use change is the main driver for the reductions

334 in East Asia (Fig. 6b). Increasing $[\text{CO}_2]$ promotes photosynthesis but meanwhile inhibits
335 BVOC emissions, leading to offsetting CO_2 effects on isoprene. Consequently, the global
336 isoprene emission is mainly driven by meteorological changes (Fig. 6b). In contrast,
337 using MEGAN scheme, the YIBs model simulates a global reduction of 1.1 Tg C a^{-2} for
338 isoprene emissions (Fig. 6c). Strong declines are found in the tropical rainforest, for
339 example in the Amazon ($-0.43 \text{ Tg C a}^{-2}$), central Africa ($-0.14 \text{ Tg C a}^{-2}$), and Indonesia ($-$
340 0.16 Tg C a^{-2}) (Fig. 6c). The MEGAN scheme is sensitive to both light and temperature
341 (Guenther et al., 1995). The strong positive brightening trends in PAR in Europe (Fig.
342 S1b) promote isoprene emissions there. The positive impacts of NH warming (Fig. S1a)
343 are compensated by CO_2 inhibition, leading to small changes in isoprene emissions (Fig.
344 6c). In the tropical areas, where trends of temperature and PAR are limited, CO_2
345 inhibition results in strong reductions of BVOC emissions. Monoterpene emissions show
346 a global reduction of 0.04 Tg C a^{-2} over the past 3 decades (Fig. 6e).

347

348 **3.4 Feedback of biospheric changes to the trends**

349

350 Due to the changing climate and CO_2 fertilization, the biosphere is experiencing
351 significant changes in the past 3 decades. The most evident alterations include LAI
352 changes in peak season and phenological changes in growing and falling seasons. In this
353 section, we explore the feedback of these biospheric changes to the carbon uptake and
354 BVOC emissions.

355

356 **3.4.1 Impacts of LAI changes**

357

358 Sensitivity run LAI_ONLY retains the trends in LAI but prescribes other forcings. In this
359 simulation, trends in GPP (Fig. S2a) and NPP (Fig. S2c) generally follow that in LAI
360 (Fig. 1b), but with smaller magnitude relative to those in control simulations (Figs. 2a
361 and 2c). LAI in the north of 30°N shows widespread increases in both observations and
362 simulations (Figs. 1a and 1b). Over these northern lands, the unit change in leaf area
363 leads to enhancement of regional GPP by 32 Pg C a^{-1} , much lower than the response of
364 $116 \text{ Pg C a}^{-1} \text{ LAI}^{-1}$ for the simulation including CO_2 fertilization and climate forcings

365 (Fig. 7a). In the tropical areas, both positive and negative LAI trends are predicted due to
366 the competition between CO₂ fertilization and drought effects (Fig. 1). As a result, LAI-
367 induced GPP and NPP changes show patchy distributions at tropics (Fig. S2a and S2c),
368 leading to moderate changes in the global carbon assimilations (Table 3).

369

370 Trends in isoprene emission (calculated with the PS_BVOC scheme) also follow that of
371 LAI, except that leaf expansion results in decreased emissions at high latitudes (~60°N,
372 Fig. S2e). The cause for such inconsistency is unclear, but might be because the denser
373 leaves reduce radiation penetrating to lower canopy layers. Such impact would only
374 affect BVOC emissions at high latitudes because PAR is usually limiting near subarctic
375 areas. In most of the subtropical areas, increased LAI leads to enhanced isoprene
376 emissions. On average, unit change in LAI at north of 30°N leads to enhanced isoprene
377 emissions by 43 Tg C a⁻², only 25% of the magnitude in simulation CO₂_MET (Fig. 7b).
378 A similar ratio of 23% is achieved for MEGAN isoprene emissions. These results are
379 consistent with that for GPP (Fig. 7a), suggesting that CO₂ fertilization and
380 meteorological changes are the main drivers for the changes in carbon uptake and BVOC
381 emissions, even over the northern lands where the most evident changes in LAI are
382 observed.

383

384 **3.4.2 Impacts of phenological changes**

385

386 Plant phenology, which is the timing of budburst and leaf fall, is closely related to
387 temperature, moisture, and photoperiod and thus is experiencing significant changes in
388 the past decades following climate change (Jeong et al., 2011; Keenan et al., 2014;
389 Buitenwerf et al., 2015; Yue et al., 2015). Extension of the growing season has the
390 potential to promote carbon uptake of forests (e.g., Piao et al., 2007; Richardson et al.,
391 2009). Yet such inference requires careful interpretation because the phenological
392 changes are usually accompanied with warming and elevated [CO₂], both of which are
393 also contributing to the enhancement of carbon fluxes. Phenological changes are also
394 expected to affect BVOC emissions, however, such investigations are still missing
395 (Richardson et al., 2013). With the YIBs model, we evaluate the impacts of the growing

396 season extension on both carbon uptake and BVOC emissions by isolating long-term
397 phenological trends from changes in temperature and [CO₂].

398

399 The YIBs model simulates advanced spring and delayed autumn over most areas in NH
400 (Fig. S3). Budburst dates advance on average by 0.16 days a⁻¹ in Europe and 0.15 days a⁻¹
401 in East Asia (Table 2), but with moderate changes or even delays in northwestern Asia
402 and eastern Siberia (Fig. S3a). Spring is earlier by 0.14 days a⁻¹ in eastern U.S. while
403 delayed by 0.15 days a⁻¹ in northwestern U.S. and southeastern Canada, leading to a
404 minor advance of 0.01 days a⁻¹ over North America. Dormancy onset dates are largely
405 delayed in eastern Europe and northwestern Asia (~0.3 day a⁻¹), western U.S. (~0.1 day a⁻¹)
406 ¹), boreal Canada (~0.1 day a⁻¹), and northeastern China (~0.1 day a⁻¹) (Fig. S3b).
407 Advanced autumn (~0.1 day a⁻¹) is predicted in northern Asia. Most of these changes are
408 consistent with observations from remote sensing data (Jeong et al., 2011), except for
409 some discrepancies in the magnitude. The predicted phenological trends mainly follow
410 the long-term changes of surface air temperature, especially that in April (for spring) and
411 September (for autumn) (Fig. S4). Sensitivity tests without chilling requirement and
412 photoperiod limit show similar changes (Yue et al., 2015), suggesting that temperature
413 changes dominantly drive the trends of forest phenology in the past 3 decades.

414

415 On average, the YIBs model simulates advanced budburst by 0.12 day a⁻¹ and delayed
416 dormancy onset by 0.09 day a⁻¹ at north of 30°N in the past 3 decades (Figs. 8a and 8b).
417 Observations based on remote sensing greenness show trends of -0.11 day a⁻¹ for onset
418 and 0.25 day a⁻¹ for offset during 1990-2009 (Zhu et al., 2013). An ensemble prediction
419 based on 9 terrestrial models yields an advance of 0.08 ± 0.13 day a⁻¹ for onset and a
420 delay of 0.22 ± 0.1 day a⁻¹ for offset (Sitch et al., 2015). Our predictions are in broad
421 agreement with these estimates though the autumn delay is less, likely because the
422 positive trend of offset is weaker for the recent decade (Jeong et al., 2011).

423

424 We plot the annual total GPP and isoprene emissions at north of 30°N against the length
425 of growing season for 1982-2011 (Figs. 8c and 8d). In the CO₂_MET run, the 1-day
426 extension is correspondent to increases of 0.17 Pg C a⁻¹ in GPP and 0.34 Tg C a⁻¹ in

427 isoprene emissions. If only temperature is allowed to vary, the phenological trend
428 remains the same while the increases of GPP and isoprene emissions are largely
429 weakened. In the TEMP_ONLY run, the 1-day extension in growing season is
430 accompanied by increases of 0.05 Pg C a⁻¹ in GPP and 0.25 Tg C a⁻¹ in isoprene
431 emissions. The changes in BVOC emissions are not as dramatic as those of GPP because
432 CO₂ has both enhancing and suppressing impacts on the former. If we further exclude
433 temperature effects (PHEN_ONLY run), GPP increases only by 0.01 Pg C a⁻¹ while
434 isoprene emissions decrease by 0.1 Tg C a⁻¹, both of which are not statistically
435 significant, suggesting that the phenological change alone does not promote either GPP
436 or isoprene emissions. There are two reasons for this apparent contradiction. First, the
437 extension of the growing season occurs in shoulder months, usually in May and
438 September, when both GPP and BVOC emissions and their changes are much smaller
439 compared to that in peak months (Fig. S5). Second, phenological changes are not uniform
440 in space. As Fig. S3 shows, both positive and negative changes are predicted for budburst
441 and dormancy onset dates. Such spatial inhomogeneity, in combination with the
442 discrepancies in regional vegetation types and meteorological conditions, result in varied
443 responses in GPP (Fig. S2b) and isoprene emissions (Fig. S2f).

444

445 Plant phenology at lower latitudes (30°S-30°N) is also experiencing dramatic changes,
446 though such changes are diverse in phase, magnitude, or both (Buitenwerf et al., 2015).
447 In the model, tropical phenology is mainly driven by soil wetness and as a result exhibits
448 large changes in the past 3 decades (not shown). These changes lead to a reduction of 42
449 Tg C a⁻¹ in GPP at the tropics (Fig. S2b), which accounts for 14% of global GPP trend
450 but with the opposite sign (Table 3), suggesting additional inhibition of drought on
451 carbon cycle. A similar conclusion applies for BVOC emissions (Fig. S2f), though
452 experiments suggest that isoprene production has some tolerance to mild drought
453 conditions (e.g., Pegoraro et al., 2006). However, changes in drought-dependent
454 phenology are very uncertain and observations are not available for evaluation. We
455 assume that phenological changes may have larger impacts on both carbon assimilation
456 and BVOC emissions at tropical areas than that at higher latitudes.

457

458

459 **4 Discussion**

460

461 **4.1 Uncertainties in observations**

462

463 Terrestrial biosphere modeling is a useful tool to identify drivers of long-term changes in
464 land carbon fluxes. The reliability of simulations is dependent on the availability of
465 observations for model validation. In this study, we use 30-year LAI observations from
466 the LAI3g product (Zhu et al., 2013) and 12-year GPP from MODIS (Zhao et al., 2005),
467 both of which are remote sensing retrievals, to validate the simulated trends (Figs. 1 and
468 3). We found the offline global model biases against both fields, especially for LAI (Fig.
469 1). Such discrepancies may in part result from the uncertainties in measurements
470 themselves. As a check, we compare the derived LAI trends from LAI3g with retrievals
471 from MODIS for the overlap period of 2000-2011 (Figs. S6a and S6b). Global LAI
472 significantly increases in LAI3g but show widespread reductions in MODIS, especially
473 over subtropical areas. Simulated trends (CO2_LUC_MET) are closer to the estimates
474 with MODIS, especially for the changes in the NH (not shown). Meanwhile, we compare
475 the derived GPP trends from MODIS with that upscaled from FLUXNET data using an
476 ensemble of regression trees (Jung et al., 2009) for 2000-2011 (Figs. S6c and S6d). The
477 two products show similar trends over most areas except for some discrepancies in
478 tropical areas and the eastern U.S. Simulated GPP trends match results from Jung et al.
479 (2009) better than that from MODIS (Fig. 3a). However, we do not use Jung et al. (2009)
480 to validate simulations for 1982-2011 because the earliest flux tower observations began
481 only in middle 1990s. The large discrepancies in the observed trends among different
482 data sets not only indicate the importance of model evaluations with multiple products,
483 but also put forward the necessity of data inter-comparisons and algorithm improvements
484 to alleviate uncertainties in observations.

485

486 **4.2 Comparisons with other modeling studies**

487

488 | We assess the YIBs simulations within the context of other models and/or previous multi-
489 | model studies to evaluate the robustness of the predicted trends in land carbon fluxes and
490 | BVOC emissions. The YIBs model predicts NPP trends of 67.4 Tg C a⁻² in northern land
491 | (25-90°N) and 98.1 Tg C a⁻² in tropical land (15°S-25°N), similar to the ensemble
492 | estimates of 63 ± 22 and 102 ± 34 Tg C a⁻² for 1990-2009 based on 9 terrestrial biosphere
493 | models (Sitch et al., 2015). However, the simulated NPP trend is only 19.8 Tg C a⁻² in
494 | southern land (15-90°S), much lower than the ensemble mean value of 53 ± 31 Tg C a⁻²
495 | in Sitch et al. (2015). As for the NEP, the YIBs predicts trends of 2.0 Tg C a⁻² in northern
496 | land, 1.0 Tg C a⁻² in tropical land, and -0.3 Tg C a⁻² in southern land, much smaller in
497 | magnitude compared with the -2.0 ± 12, 36.0 ± 13, and 21 ± 17 Tg C a⁻² estimated by
498 | Sitch et al. (2015). However, their predictions are insignificant ($p > 0.05$) for 9, 5, and 7
499 | out of 9 models in the northern, tropical, and southern land respectively, suggesting that
500 | the strengthening uptake by terrestrial ecosystem is not robust.

501 |
502 | For the BVOC, Stavrakou et al. (2014) investigated isoprene emissions over Asia during
503 | 1979-2012 using the MEGAN scheme and taking into account both climate and land-use
504 | changes. Their results showed widespread increases in the emissions over China but
505 | moderate decreases in Indonesia. In contrast, the YIBs model with the MEGAN scheme
506 | simulates widespread reductions in the same areas for 1980-2011 (Fig. 6c). The
507 | discrepancies between studies are accounted for by differences in the drivers including
508 | land cover change, meteorology, and CO₂ inhibition effects. The YIBs model is driven
509 | with land cover data from Hurtt et al. (2011), which estimates an increase of crop (non-
510 | isoprene emitter) fraction in East China by 0.32% per year in the last 3 decades, at the
511 | cost of the coverage loss by 0.12% a⁻¹ for DBF and 0.14% a⁻¹ for ENF (strong BVOC
512 | emitters). However, the data from Ramankutty and Foley (1999), used by Stavrakou et al.
513 | (2014) with updates to 2007, show a reduction of the crop fraction over East China for
514 | the similar period. In addition, the ERA-Interim PAR used in Stavrakou et al. (2014)
515 | shows an increasing trend in southeast China (c.f. their Fig. 5c). On the contrary, the
516 | WFDEI PAR for YIBs exhibits a declining trend in the same region (Fig. S1b), leading to
517 | a reduction in isoprene emissions. The WFDEI surface solar radiation is based on the
518 | ERA-Interim radiation but is adjusted using the average cloud cover from the Climatic

Xu Yue 10/10/15 6:48 PM

Deleted: Stavrakou et al. (2014)

520 Research Unit (CRU) and taking into account the effects of interannual changes in
521 atmospheric aerosols (Weedon et al., 2011). Finally, the YIBs simulations include CO₂
522 inhibition effects on BVOC emissions, which were neglected in Stavrakou et al. (2014).

523

524 Naik et al. (2004) predicted a global trend of 1.3 Tg C a⁻² for isoprene emissions during
525 1971-1990 using the Integrated Biospheric Simulator (IBIS) driven with monthly mean
526 CRU meteorology. Lathiere et al. (2006) estimated an increasing global trend of 0.3 Tg C
527 a⁻² for 1983-1995 using the ORCHIDEE (Organizing Carbon and Hydrology in Dynamic
528 EcosystEms) vegetation model driven with sub-daily variables from the NCEP/DOE
529 (National Center for Environmental Predictions/Department of Energy) Reanalysis 2.
530 Muller et al. (2008) reported a global increase of 4.5 Tg C a⁻² for 1995-2006 using a
531 canopy environmental model and the NCEP meteorological data. In contrast to these
532 previous studies, YIBs with the MEGAN scheme simulates a decreasing trend of ~1 Tg C
533 a⁻² in the past 3 decades. The main cause of the discrepancy in the sign of change is the
534 missing CO₂ inhibition effects in the previous studies. In addition, differences in
535 vegetation models, meteorological forcings, and time frames of investigation also likely
536 contribute. The YIBs result is consistent with a recent study by Sindelarova et al. (2014),
537 who reported a decreasing trend of ~1.2 Tg C a⁻² for global isoprene emissions during
538 1980-2010 using the MEGAN scheme and inclusion of a CO₂ inhibition parameterization
539 from Heald et al. (2009).

540

541 **4.3 Impacts of CO₂ effects**

542

543 Similar to the multi-model ensemble predictions (Sitch et al., 2015), we found that global
544 trends in carbon fluxes are dominantly driven by CO₂ fertilization (Figs. 2 and 5). In the
545 YIBs, the global responses to elevated [CO₂] is 0.2% ppm⁻¹ for GPP and 0.27% ppm⁻¹ for
546 NPP, with relatively uniform spatial distribution (Figs. S7a and S7b). The GPP response
547 falls within the range of 0.05-0.21% ppm⁻¹ predicted by 10 terrestrial models (Piao et al.,
548 2013) and that of 0.01-0.32% ppm⁻¹ observed from multiple free-air CO₂ enrichment
549 (FACE) sites (Ainsworth and Long, 2005). The NPP response is higher than the model
550 ensemble of 0.16% ppm⁻¹ (Piao et al., 2013) and the observed median value of 0.13%

551 ppm⁻¹ (Norby et al., 2005), suggesting that CO₂ fertilization to NPP may be
552 overestimated in the YIBs. One possible cause is the omission of N limitation in the
553 model, which could reduce CO₂ responses by half (Piao et al., 2013). Elevated [CO₂]
554 leads to increases of 0.023 Pg C a⁻¹ ppm⁻¹ in NEP, within the multi-model range of 0.003-
555 0.06 Pg C a⁻¹ ppm⁻¹ (Piao et al., 2013).

556

557 Responses of BVOC emissions to elevated [CO₂] are different between PS_BVOC and
558 MEGAN schemes (Figs. S7c and S7d). PS_BVOC includes both CO₂ fertilization (on
559 photosynthesis) and inhibition (on isoprene) effects, leading to moderate but generally
560 positive changes in isoprene emissions. In contrast, emissions from the MEGAN scheme
561 are not dependent on foliar photosynthesis and as a result only CO₂ inhibition is enforced.
562 Chamber experiments show contrary tendencies for photosynthesis and isoprene in
563 response to elevated [CO₂] (Possell et al., 2005), supporting the simulations with
564 MEGAN. In addition, the magnitude of CO₂ inhibition implemented in MEGAN (-0.25%
565 ppm⁻¹) is close to observations (-0.26% ppm⁻¹) in Possell et al. (2005). However, most of
566 these experiments are conducted for short-term period and cannot detect LAI changes due
567 to the long-term CO₂ fertilization. In addition, the impacts of CO₂ are dependent on
568 species and environmental conditions (ambient temperature and light availability). For
569 example, Buckley (2001) found almost no responses in isoprene emissions to the elevated
570 [CO₂] for oak trees. Furthermore, experiments with high temperature and/or light density
571 show increasing isoprene at elevated [CO₂] (Sun et al., 2013). These studies suggest that
572 the real responses of isoprene emissions to CO₂ under long-term climate change may not
573 be so linear as predicted in MEGAN scheme. More sensitivity experiments and long-term
574 samplings are required to identify CO₂-isoprene relationships on broad range of biomes
575 and locations.

576

577 **4.4 Impacts of meteorology**

578

579 Predicted long-term trends show large deviations against observations at tropical areas
580 (Fig. 3), where meteorology plays important and complex roles. Responses of carbon
581 fluxes to temperature are more diverse than to CO₂ (Figs. S8a and S8b). In the YIBs,

582 negative responses of GPP and NPP are predicted in tropical areas, where soil moisture
583 availability limits plant functions (e.g. stomatal conductance) to the increased
584 temperature. Furthermore, for tropical rainforests where ambient temperature is higher
585 than optimal photosynthetic temperature (25-30°C), additional warming decreases carbon
586 assimilation, especially for NPP because of simultaneous increases in plant respiration
587 (Liang et al., 2013). On the contrary, warming leads to enhanced GPP and NPP at wetter
588 and cooler areas in the NH subtropics. Such spatial pattern is consistent with multi-model
589 ensemble predictions (Piao et al., 2013). On the global scale, warming results in changes
590 of $-0.7\% \text{ } ^\circ\text{C}^{-1}$ for GPP in YIBs, falling within the range of $-1.6\text{-}1.4\% \text{ } ^\circ\text{C}^{-1}$ estimated by 10
591 models (Piao et al., 2013). Predicted NPP responses of $-15\text{-}6\% \text{ } ^\circ\text{C}^{-1}$ (Fig. S8b) is not so
592 positive as the measurements of $-8\text{-}40\% \text{ } ^\circ\text{C}^{-1}$, probably because most of current warming
593 experiments are located in subtropics of NH (Wu et al., 2011). Elevated temperature
594 changes NEP by $-1.4 \text{ Pg C a}^{-1} \text{ } ^\circ\text{C}^{-1}$, also within the multi-model range of $-5\text{-}1 \text{ Pg C a}^{-1}$
595 $^\circ\text{C}^{-1}$ (Piao et al., 2013). Simulated isoprene emissions with PS_BVOC show similar
596 warming responses as that of carbon fluxes (Fig. S8c), except for tropical rainforests
597 where the former is positive while the latter is negative. Such decoupling is attributed to
598 the differences in optimal temperatures between isoprene (35-40 °C) and photosynthesis
599 (25-30 °C). Simulations with MEGAN scheme show very strong temperature dependence
600 of $6\text{-}15\% \text{ } ^\circ\text{C}^{-1}$ (Fig. S8d), consistent with measurements of $5\text{-}20\% \text{ } ^\circ\text{C}^{-1}$ for aspen
601 (Niinemets and Sun, 2015) and $9\text{-}12\% \text{ } ^\circ\text{C}^{-1}$ for oak (Li et al., 2011). However,
602 experiments with some other species (e.g. spruce in Kivimaenpaa et al. (2013)) show no
603 responses or moderate ones, suggesting that warming sensitivity of isoprene emissions
604 might be dependent on species and ambient conditions.

605

606 Responses to PAR are mostly positive and distributed evenly, with global sensitivity of
607 $0.3\% \text{ W}^{-1} \text{ m}^2$ for GPP and $0.5\% \text{ W}^{-1} \text{ m}^2$ for NPP (Figs. S9a and S9b). Isoprene emissions
608 from both PS_BVOC and MEGAN schemes show similar responses to PAR, with larger
609 sensitivity in subtropics than that in tropics (Figs. S9c and S9d), likely because the
610 ambient PAR is higher at lower latitude, leading to slower responses of isoprene
611 emissions to the unit changes of light (Guenther et al., 1993). YIBs simulations show that

612 PAR is not the driver of long-term trends in carbon fluxes and BVOC emissions (Fig. 4),
613 likely because changes in solar radiation is limited in the past 3 decades (Figs. S1b).

614

615 Soil moisture dominates climate-driven flux changes in tropical areas (Fig. 4). In YIBs
616 model, changes in soil water availability affect carbon assimilation through the alteration
617 of leaf stomatal conductance and plant phenology (especially for shrublands and
618 grasslands in arid regions). Both GPP and NPP show strong responses to soil wetness
619 variations, especially over tropics where >10% changes are found for every increase of
620 0.01 in soil wetness at 1.5 m (Figs. S10a and S10b). On the global scale, GPP changes by
621 4.7% 0.01^{-1} and NPP by 5.5% 0.01^{-1} in response to soil wetness. Although experiments
622 also show rapid reductions in carbon assimilation due to drought stress (e.g., Ruehr et al.,
623 2012; Xia et al., 2014), the magnitude of such influence is difficult to evaluate because
624 different metrics and depths of soil water are used in measurements. Isoprene emissions
625 from PS_BVOC show similar soil-wetness responses to that of GPP (Fig. S10c),
626 indicating that drought reduces BVOC emissions. However, observations show
627 insignificant changes of isoprene with mild drought stress (e.g., Pegoraro et al., 2006),
628 though such drought tolerance is strongly weakened at severe drought and/or warm
629 conditions (Centritto et al., 2011). Consistent with these experiments, MEGAN scheme
630 does not include drought inhibition on isoprene emissions. Simulations with YIBs show
631 large responses of BVOC to soil wetness in tropical areas (Fig. S10d), mainly because of
632 the changes in drought-dependent phenology.

633

634 **4.5 Impacts of land use change**

635

636 Changes of land use show moderate impacts on global carbon budget (Fig. 2) and BVOC
637 emissions (Fig. 6) in the past 3 decades, though regional perturbations are found in China
638 and Europe. The afforestation in Europe helps promote regional carbon uptake, resulting
639 in more reasonable trends in LAI compared with remote sensing data (Fig. 1). However,
640 the expansion of crop in China leads to a reduction in LAI, which is not supported by the
641 satellite data. One possible cause is the uncertainty in crop fraction, because data from
642 Hurtt et al. (2011), used by YIBs, show crop expansion while data from Ramankutty and

643 Foley (1999) suggest reductions of the crop fraction over East China over the similar
644 period. The role of land use change in our simulation might be conservative because we
645 consider only land cover changes. Perturbed emissions from land use management, such
646 as forest lodging, cropping practice, use of fertilizer, fire management and so on
647 (Houghton, 2010) may alter regional carbon budget by changing carbon sinks to sources.
648 Studies including gross emissions of land use perturbation estimated a global net land
649 source to atmosphere, which shows decreasing trend in the last 3 decades (Ciais et al.,
650 2013). Such change may help strengthen net land carbon sink but is missing in our study.

651

652 **4.6 Impacts of biospheric changes**

653

654 The land biosphere has experienced significant changes in the past 3 decades. At north of
655 30°N, changes in LAI account for 25% of the trends in regional carbon fluxes and
656 isoprene emissions. However, the extension of growing season alone makes insignificant
657 contributions to the increased carbon assimilation. This conclusion is inconsistent with
658 site-level observations that show evident increases in carbon assimilation at early spring
659 and/or late autumn in recent decades (Dragoni et al., 2011; Keenan et al., 2014). The
660 causes for such discrepancies lie in two. First, phenology at specific location may exhibit
661 much more intense changes than that at larger scale. For example, Dragoni et al. (2011)
662 estimated extensions of growing season by 2.3-3.3 day a⁻¹ in Morgan-Monroe State
663 Forest in south-central Indiana of US for 1998-2008. The magnitude of this change is ~10
664 times larger than the observed value of 0.36 day a⁻¹ from satellite and simulated value of
665 0.22 day a⁻¹ with YIBs for the northern lands. Second, enhanced temperature also
666 contributes to the stronger uptake at early spring and late autumn. One difficulty for the
667 observation-based estimate of phenological impacts is that extension of growing season is
668 accompanied by warmer climate, which may stimulate both carbon assimilation and
669 BVOC production. In a recent study, Barlow et al. (2015) found invariant length of land
670 carbon uptake period at high northern latitudes based on the first time differential of
671 atmospheric CO₂ concentrations, suggesting that increased greenness is not necessarily
672 equal to enhanced carbon uptake in shoulder seasons. Furthermore, Barlow et al. (2015)
673 showed that enhanced peak uptake is the main driver for the strengthened carbon sink at

674 high northern latitudes over the past 4 decades. These conclusions are supportive of our
675 simulations for the monthly trends at subtropical regions (North America, Europe, and
676 East Asia) (Fig. S5).

677

678

679 **5 Conclusions**

680

681 With YIBs model, we estimated global increases of carbon assimilation especially at
682 tropical areas for 1982-2011. This trend is mainly attributed to the widespread CO₂
683 fertilization effect, and jointly affected by changes in meteorology and land cover.
684 Increase of temperature promotes carbon uptake of forest ecosystems at high latitudes
685 (>30°N) while drought tendency dampens GPP and NPP of grasslands and shrublands at
686 low latitudes (30°S-30°N). The widespread increases of LAI at northern lands account for
687 ~25% of the regional GPP trends. Significant changes in phenology are found at north of
688 30°N; however, this temperature-driven phenological change alone is not promoting
689 regional carbon assimilation. Changes in land use show limited influences on global
690 carbon fluxes, except for some regional impacts over Europe (afforestation) and China
691 (deforestation). Due to the simultaneous enhancement in soil respiration, land carbon sink
692 has remained almost stable in the past 3 decades. The YIBs model does not yet include a
693 fully coupled carbon-nitrogen cycle, thus the model may overestimate CO₂ fertilization
694 effects. On the contrary, implementation of drought-dependent phenology may amplify
695 drought inhibition effects on photosynthesis and result in an underestimation of carbon
696 uptake.

697

698 We estimated global trends of BVOC emissions with two schemes. Simulations with
699 PS_BVOC scheme show increasing isoprene emissions, mainly attributed to the increases
700 of temperature. For this scheme, CO₂ effects are neutralized due to both fertilization (on
701 photosynthesis) and inhibition (on isoprene). Simulations with MEGAN scheme show
702 decreasing emissions of isoprene and monoterpene because of CO₂ inhibition, especially
703 in the tropics. In subtropical areas, both schemes predict regional increases of BVOC

704 emissions in Europe following the warming trend and afforestation, but reductions in the
705 U.S. and China due to cropland expansion.

706

707

708 *Acknowledgements.* Funding support for this research is provided by the NASA
709 Atmospheric Composition Campaign Data Analysis and Modeling Program. This project
710 was supported in part by the facilities and staff of the Yale University Faculty of Arts and
711 Sciences High Performance Computing Center.

712

713

714 **References**

- 715 Ainsworth, E. A., and Long, S. P.: What have we learned from 15 years of free-air CO₂
716 enrichment (FACE)? A meta-analytic review of the responses of photosynthesis,
717 canopy, *New Phytol*, 165, 351-371, doi:10.1111/J.1469-8137.2004.01224.X, 2005.
- 718 Arneth, A., Niinemets, U., Pressley, S., Back, J., Hari, P., Karl, T., Noe, S., Prentice, I.
719 C., Serca, D., Hickler, T., Wolf, A., and Smith, B.: Process-based estimates of
720 terrestrial ecosystem isoprene emissions: incorporating the effects of a direct CO₂-
721 isoprene interaction, *Atmos Chem Phys*, 7, 31-53, doi:10.5194/acp-7-31-2007, 2007.
- 722 Barlow, J. M., Palmer, P. I., Bruhwiler, L. M., and and Tans, P.: Analysis of CO₂ mole
723 fraction data: first evidence of large-scale changes in CO₂ uptake at high northern
724 latitudes, *Atmos. Chem. Phys. Discuss.*, 15, 7089-7139, doi:10.5194/acpd-15-7089-
725 2015, 2015.
- 726 Beer, C., Reichstein, M., Tomelleri, E., Ciais, P., Jung, M., Carvalhais, N., Rodenbeck,
727 C., Arain, M. A., Baldocchi, D., Bonan, G. B., Bondeau, A., Cescatti, A., Lasslop, G.,
728 Lindroth, A., Lomas, M., Luyssaert, S., Margolis, H., Oleson, K. W., Rouspard, O.,
729 Veenendaal, E., Viovy, N., Williams, C., Woodward, F. I., and Papale, D.: Terrestrial
730 Gross Carbon Dioxide Uptake: Global Distribution and Covariation with Climate,
731 *Science*, 329, 834-838, doi:10.1126/Science.1184984, 2010.
- 732 Buckley, P. T.: Isoprene emissions from a Florida scrub oak species grown in ambient
733 and elevated carbon dioxide, *Atmos Environ*, 35, 631-634, doi:10.1016/S1352-
734 2310(00)00332-0, 2001.
- 735 Buitenwerf, R., Rose, L., and Higgins, S. I.: Three decades of multi-dimensional change
736 in global leaf phenology, *Nat Clim Change*, 5, 364-368, 2015.
- 737 Carslaw, K. S., Boucher, O., Spracklen, D. V., Mann, G. W., Rae, J. G. L., Woodward,
738 S., and Kulmala, M.: A review of natural aerosol interactions and feedbacks within
739 the Earth system, *Atmos. Chem. Phys.*, 10, 1701-1737, doi:10.5194/acp-10-1701-
740 2010, 2010.
- 741 Centritto, M., Brilli, F., Fodale, R., and Loreto, F.: Different sensitivity of isoprene
742 emission, respiration and photosynthesis to high growth temperature coupled with
743 drought stress in black poplar (*Populus nigra*) saplings, *Tree Physiol*, 31, 275-286,
744 doi:10.1093/Treephys/Tpql12, 2011.
- 745 Ciais, P., Sabine, C., Bala, G., Bopp, L., Brovkin, V., Canadell, J., Chhabra, A., DeFries,
746 R., Galloway, J., Heimann, M., Jones, C., Le Quere, C., Myneni, R., Piao, S., and
747 Thornton, P.: Carbon and other biogeochemical cycles, in: *Climate Change 2013: The*
748 *Physical Science Basis. Contribution of Working Group I to the Fifth Assessment*
749 *Report of the Intergovernmental Panel on Climate Change*, edited by: Stocker, T. F.,
750 Qin, D., Plattner, G.-K., Tignor, M., Allen, S. K., Boschung, J., Nauels, A., Xia, Y.,
751 Bex, V., and Midgley, P. M., Cambridge University Press, Cambridge, United
752 Kingdom and New York, NY, USA, 465-570, 2013.
- 753 Collatz, G. J., Ball, J. T., Grivet, C., and Berry, J. A.: Physiological and Environmental-
754 Regulation of Stomatal Conductance, Photosynthesis and Transpiration - a Model
755 That Includes a Laminar Boundary-Layer, *Agr Forest Meteorol*, 54, 107-136,
756 doi:10.1016/0168-1923(91)90002-8, 1991.
- 757 Cox, P. M.: Description of the "TRIFFID" Dynamic Global Vegetation Model, Hadley
758 Centre technical note 24, Berks, UK, 2001.

- 759 Defries, R. S., Hansen, M. C., Townshend, J. R. G., Janetos, A. C., and Loveland, T. R.:
 760 A new global 1-km dataset of percentage tree cover derived from remote sensing,
 761 Global Change Biol, 6, 247-254, doi:10.1046/J.1365-2486.2000.00296.X, 2000.
- 762 Dragoni, D., Schmid, H. P., Wayson, C. A., Potter, H., Grimmond, C. S. B., and
 763 Randolph, J. C.: Evidence of increased net ecosystem productivity associated with a
 764 longer vegetated season in a deciduous forest in south-central Indiana, USA, Global
 765 Change Biol, 17, 886-897, doi:10.1111/J.1365-2486.2010.02281.X, 2011.
- 766 Farquhar, G. D., Caemmerer, S. V., and Berry, J. A.: A Biochemical-Model of
 767 Photosynthetic Co2 Assimilation in Leaves of C-3 Species, Planta, 149, 78-90,
 768 doi:10.1007/Bf00386231, 1980.
- 769 Guenther, A. B., Zimmerman, P. R., Harley, P. C., Monson, R. K., and Fall, R.: Isoprene
 770 and Monoterpene Emission Rate Variability - Model Evaluations and Sensitivity
 771 Analyses, J. Geophys. Res., 98, 12609-12617, doi:10.1029/93jd00527, 1993.
- 772 Guenther, A. B., Hewitt, C. N., Erickson, D., Fall, R., Geron, C., Graedel, T., Harley, P.,
 773 Klinger, L., Lerdau, M., McKay, W. A., Pierce, T., Scholes, B., Steinbrecher, R.,
 774 Tallamraju, R., Taylor, J., and Zimmerman, P.: A Global-Model of Natural Volatile
 775 Organic-Compound Emissions, J. Geophys. Res., 100, 8873-8892,
 776 doi:10.1029/94jd02950, 1995.
- 777 [Guenther, A. B., Jiang, X., Heald, C. L., Sakulyanontvittaya, T., Duhl, T., Emmons, L.](#)
 778 [K., and Wang, X.: The Model of Emissions of Gases and Aerosols from Nature](#)
 779 [version 2.1 \(MEGAN2.1\): an extended and updated framework for modeling biogenic](#)
 780 [emissions, Geosci Model Dev, 5, 1471-1492, doi:10.5194/Gmd-5-1471-2012, 2012.](#)
- 781 Hansen, M. C., DeFries, R. S., Townshend, J. R. G., Carroll, M., Dimiceli, C., and
 782 Sohlberg, R. A.: Global Percent Tree Cover at a Spatial Resolution of 500 Meters:
 783 First Results of the MODIS Vegetation Continuous Fields Algorithm, Earth Interact,
 784 7, [1-15, doi:10.1175/1087-3562\(2003\)007<0001:GPTCAA>2.0.CO;2, 2003.](#)
- 785 Heald, C. L., Wilkinson, M. J., Monson, R. K., Alo, C. A., Wang, G. L., and Guenther,
 786 A.: Response of isoprene emission to ambient CO2 changes and implications for
 787 global budgets, Global Change Biol, 15, 1127-1140, doi:10.1111/J.1365-
 788 2486.2008.01802.X, 2009.
- 789 Heinsch, F. A., Zhao, M. S., Running, S. W., Kimball, J. S., Nemani, R. R., Davis, K. J.,
 790 Bolstad, P. V., Cook, B. D., Desai, A. R., Ricciuto, D. M., Law, B. E., Oechel, W. C.,
 791 Kwon, H., Luo, H. Y., Wofsy, S. C., Dunn, A. L., Munger, J. W., Baldocchi, D. D.,
 792 Xu, L. K., Hollinger, D. Y., Richardson, A. D., Stoy, P. C., Siqueira, M. B. S.,
 793 Monson, R. K., Burns, S. P., and Flanagan, L. B.: Evaluation of remote sensing based
 794 terrestrial productivity from MODIS using regional tower eddy flux network
 795 observations, Ieee T Geosci Remote, 44, 1908-1925, doi:10.1109/Tgrs.2005.853936,
 796 2006.
- 797 Houghton, R. A.: How well do we know the flux of CO2 from land-use change?, Tellus
 798 B, 62, 337-351, doi:Doi 10.1111/J.1600-0889.2010.00473.X, 2010.
- 799 Hurtt, G. C., Chini, L. P., Frolking, S., Betts, R. A., Feddema, J., Fischer, G., Fisk, J. P.,
 800 Hibbard, K., Houghton, R. A., Janetos, A., Jones, C. D., Kindermann, G., Kinoshita,
 801 T., Goldewijk, K. K., Riahi, K., Shevliakova, E., Smith, S., Stehfest, E., Thomson, A.,
 802 Thornton, P., van Vuuren, D. P., and Wang, Y. P.: Harmonization of land-use
 803 scenarios for the period 1500-2100: 600 years of global gridded annual land-use

Xu Yue 10/10/15 6:48 PM

Deleted: 2003.

805 transitions, wood harvest, and resulting secondary lands, *Climatic Change*, 109, 117-
806 161, doi:10.1007/S10584-011-0153-2, 2011.

807 Jeong, S. J., Ho, C. H., Gim, H. J., and Brown, M. E.: Phenology shifts at start vs. end of
808 growing season in temperate vegetation over the Northern Hemisphere for the period
809 1982-2008, *Global Change Biol*, 17, 2385-2399, doi:10.1111/J.1365-
810 2486.2011.02397.X, 2011.

811 Jung, M., Reichstein, M., and Bondeau, A.: Towards global empirical upscaling of
812 FLUXNET eddy covariance observations: validation of a model tree ensemble
813 approach using a biosphere model, *Biogeosciences*, 6, 2001-2013, doi:10.5194/bg-6-
814 2001-2009, 2009.

815 Keenan, T. F., Gray, J., Friedl, M. A., Toomey, M., Bohrer, G., Hollinger, D. Y.,
816 Munger, J. W., O'Keefe, J., Schmid, H. P., SueWing, I., Yang, B., and Richardson, A.
817 D.: Net carbon uptake has increased through warming-induced changes in temperate
818 forest phenology, *Nat Clim Change*, 4, 598-604, doi:10.1038/Nclimate2253, 2014.

819 Kivimaenpaa, M., Riikonen, J., Ahonen, V., Tervahauta, A., and Holopainen, T.:
820 Sensitivity of Norway spruce physiology and terpenoid emission dynamics to
821 elevated ozone and elevated temperature under open-field exposure, *Environ Exp*
822 *Bot*, 90, 32-42, doi:10.1016/J.Envexpbot.2012.1t004, 2013.

823 Lathiere, J., Hauglustaine, D. A., Friend, A. D., De Noblet-Ducoudre, N., Viovy, N., and
824 Folberth, G. A.: Impact of climate variability and land use changes on global biogenic
825 volatile organic compound emissions, *Atmos Chem Phys*, 6, 2129-2146,
826 doi:10.5194/acp-6-2129-2006, 2006.

827 Le Quere, C., Raupach, M. R., Canadell, J. G., Marland, G., Bopp, L., Ciais, P., Conway,
828 T. J., Doney, S. C., Feely, R. A., Foster, P., Friedlingstein, P., Gurney, K., Houghton,
829 R. A., House, J. I., Huntingford, C., Levy, P. E., Lomas, M. R., Majkut, J., Metzl, N.,
830 Ometto, J. P., Peters, G. P., Prentice, I. C., Randerson, J. T., Running, S. W.,
831 Sarmiento, J. L., Schuster, U., Sitch, S., Takahashi, T., Viovy, N., van der Werf, G.
832 R., and Woodward, F. I.: Trends in the sources and sinks of carbon dioxide, *Nat*
833 *Geosci*, 2, 831-836, doi:10.1038/Ngeo689, 2009.

834 Li, Z. R., Ratliff, E. A., and Sharkey, T. D.: Effect of Temperature on Postillumination
835 Isoprene Emission in Oak and Poplar, *Plant Physiol*, 155, 1037-1046,
836 doi:10.1104/Pp.110.167551, 2011.

837 Liang, J. Y., Xia, J. Y., Liu, L. L., and Wan, S. Q.: Global patterns of the responses of
838 leaf-level photosynthesis and respiration in terrestrial plants to experimental warming,
839 *J Plant Ecol*, 6, 437-447, doi:10.1093/Jpe/Rtt003, 2013.

840 Mao, J. F., Shi, X. Y., Thornton, P. E., Hoffman, F. M., Zhu, Z. C., and Myneni, R. B.:
841 Global Latitudinal-Asymmetric Vegetation Growth Trends and Their Driving
842 Mechanisms: 1982-2009, *Remote Sens*, 5, 1484-1497, doi:Doi 10.3390/Rs5031484,
843 2013.

844 Marais, E. A., Jacob, D. J., Kurosu, T. P., Chance, K., Murphy, J. G., Reeves, C., Mills,
845 G., Casadio, S., Millet, D. B., Barkley, M. P., Paulot, F., and Mao, J.: Isoprene
846 emissions in Africa inferred from OMI observations of formaldehyde columns,
847 *Atmos Chem Phys*, 12, 6219-6235, doi:10.5194/Acp-12-6219-2012, 2012.

848 Meinshausen, M., Smith, S. J., Calvin, K., Daniel, J. S., Kainuma, M. L. T., Lamarque, J.
849 F., Matsumoto, K., Montzka, S. A., Raper, S. C. B., Riahi, K., Thomson, A., Velders,
850 G. J. M., and van Vuuren, D. P. P.: The RCP greenhouse gas concentrations and their

851 extensions from 1765 to 2300, *Climatic Change*, 109, 213-241, doi:10.1007/S10584-
852 011-0156-Z, 2011.

853 Monson, R. K., Trahan, N., Rosenstiel, T. N., Veres, P., Moore, D., Wilkinson, M.,
854 Norby, R. J., Volder, A., Tjoelker, M. G., Briske, D. D., Karnosky, D. F., and Fall,
855 R.: Isoprene emission from terrestrial ecosystems in response to global change:
856 minding the gap between models and observations, *Philos T R Soc A*, 365, 1677-
857 1695, doi:10.1098/Rsta.2007.2038, 2007.

858 Muller, J. F., Stavrakou, T., Wallens, S., De Smedt, I., Van Roozendael, M., Potosnak,
859 M. J., Rinne, J., Munger, B., Goldstein, A., and Guenther, A. B.: Global isoprene
860 emissions estimated using MEGAN, ECMWF analyses and a detailed canopy
861 environment model, *Atmos Chem Phys*, 8, 1329-1341, 2008.

862 Naik, V., Delire, C., and Wuebbles, D. J.: Sensitivity of global biogenic isoprenoid
863 emissions to climate variability and atmospheric CO₂, *J. Geophys. Res.*, 109,
864 D06301, doi:10.1029/2003jd004236, 2004.

865 Niinemets, U., [Tenhunen, J. D., Harley, P. C., and Steinbrecher, R.: A model of isoprene](#)
866 [emission based on energetic requirements for isoprene synthesis and leaf](#)
867 [photosynthetic properties for Liquidambar and Quercus](#), *Plant Cell Environ*, 22,
868 1319-1335, doi:10.1046/j.1365-3040.1999.00505.x, 1999.

869 Niinemets, U., and Sun, Z. H.: How light, temperature, and measurement and growth
870 [CO₂] interactively control isoprene emission in hybrid aspen, *J Exp Bot*, 66, 841-
871 851, doi:10.1093/Jxb/Eru443, 2015.

872 Norby, R. J., DeLucia, E. H., Gielen, B., Calfapietra, C., Giardina, C. P., King, J. S.,
873 Ledford, J., McCarthy, H. R., Moore, D. J. P., Ceulemans, R., De Angelis, P., Finzi,
874 A. C., Karnosky, D. F., Kubiske, M. E., Lukac, M., Pregitzer, K. S., Scarascia-
875 Mugnozza, G. E., Schlesinger, W. H., and Oren, R.: Forest response to elevated CO₂
876 is conserved across a broad range of productivity, *P Natl Acad Sci USA*, 102, 18052-
877 18056, doi:10.1073/Pnas.0509478102, 2005.

878 Oleson, K. W., Lawrence, D. M., Bonan, G. B., Drewniak, B., Huang, M., Koven, C. D.,
879 Levis, S., Li, F., Riley, W. J., Subin, Z. M., Swenson, S. C., Thornton, P. E.,
880 Bozbiyik, A., Fisher, R., Heald, C. L., Kluzek, E., Lamarque, J-F., Lawrence, P. J.,
881 Leung, L. R., Lipscomb, W., Muszala, S., Ricciuto, D. M., Sacks, W., Sun, Y., Tang,
882 J., and Yang, Z.-L.: Technical Description of version 4.5 of the Community Land
883 Model (CLM), National Center for Atmospheric Research, Boulder, CONCAR
884 Technical Note NCAR/TN-478+STR, 434, 2013.

885 Palmer, P. I., Abbot, D. S., Fu, T. M., Jacob, D. J., Chance, K., Kurosu, T. P., Guenther,
886 A., Wiedinmyer, C., Stanton, J. C., Pilling, M. J., Pressley, S. N., Lamb, B., and
887 Sumner, A. L.: Quantifying the seasonal and interannual variability of North
888 American isoprene emissions using satellite observations of the formaldehyde
889 column, *J Geophys Res-Atmos*, 111, D12315, doi:10.1029/2005jd006689, 2006.

890 Pan, Y. D., Birdsey, R. A., Fang, J. Y., Houghton, R., Kauppi, P. E., Kurz, W. A.,
891 Phillips, O. L., Shvidenko, A., Lewis, S. L., Canadell, J. G., Ciais, P., Jackson, R. B.,
892 Pacala, S. W., McGuire, A. D., Piao, S. L., Rautiainen, A., Sitch, S., and Hayes, D.: A
893 Large and Persistent Carbon Sink in the World's Forests, *Science*, 333, 988-993,
894 doi:10.1126/Science.1201609, 2011.

895 Pegoraro, E., Rey, A., Abrell, L., Vanharen, J., and Lin, G. H.: Drought effect on
896 isoprene production and consumption in Biosphere 2 tropical rainforest, *Global*
897 *Change Biol*, 12, 456-469, doi:Doi 10.1111/J.1365-2486.2006.01112.X, 2006.

898 Piao, S. L., Friedlingstein, P., Ciais, P., Viovy, N., and Demarty, J.: Growing season
899 extension and its impact on terrestrial carbon cycle in the Northern Hemisphere over
900 the past 2 decades, *Global Biogeochem Cy*, 21, Gb3018, doi:10.1029/2006gb002888,
901 2007.

902 Piao, S. L., Sitch, S., Ciais, P., Friedlingstein, P., Peylin, P., Wang, X. H., Ahlstrom, A.,
903 Anav, A., Canadell, J. G., Cong, N., Huntingford, C., Jung, M., Levis, S., Levy, P. E.,
904 Li, J. S., Lin, X., Lomas, M. R., Lu, M., Luo, Y. Q., Ma, Y. C., Myneni, R. B.,
905 Poulter, B., Sun, Z. Z., Wang, T., Viovy, N., Zaehle, S., and Zeng, N.: Evaluation of
906 terrestrial carbon cycle models for their response to climate variability and to CO2
907 trends, *Global Change Biol*, 19, 2117-2132, doi:10.1111/Gcb.12187, 2013.

908 Possell, M., Hewitt, C. N., and Beerling, D. J.: The effects of glacial atmospheric CO2
909 concentrations and climate on isoprene emissions by vascular plants, *Global Change*
910 *Biol*, 11, 60-69, doi:10.1111/J.1365-2486.2004.00889.X, 2005.

911 Ramankutty, N., and Foley, J. A.: Estimating historical changes in global land cover:
912 Croplands from 1700 to 1992, *Global Biogeochem Cy*, 13, 997-1027,
913 doi:10.1029/1999gb900046, 1999.

914 Richardson, A. D., Hollinger, D. Y., Dail, D. B., Lee, J. T., Munger, J. W., and O'Keefe,
915 J.: Influence of spring phenology on seasonal and annual carbon balance in two
916 contrasting New England forests, *Tree Physiol*, 29, 321-331, doi:Doi
917 10.1093/Treephys/Tpn040, 2009.

918 Richardson, A. D., [Anderson, R. S., Arain, M. A., Barr, A. G., Bohrer, G., Chen, G. S.,](#)
919 [Chen, J. M., Ciais, P., Davis, K. J., Desai, A. R., Dietze, M. C., Dragoni, D., Garrity,](#)
920 [S. R., Gough, C. M., Grant, R., Hollinger, D. Y., Margolis, H. A., McCaughey, H.,](#)
921 [Migliavacca, M., Monson, R. K., Munger, J. W., Poulter, B., Raczka, B. M., Ricciuto,](#)
922 [D. M., Sahoo, A. K., Schaefer, K., Tian, H. Q., Vargas, R., Verbeeck, H., Xiao, J. F.,](#)
923 [and Xue, Y. K.: Terrestrial biosphere models need better representation of vegetation](#)
924 [phenology: results from the North American Carbon Program Site Synthesis, *Global*](#)
925 [Change Biol](#), 18, 566-584, doi:10.1111/J.1365-2486.2011.02562.X, 2012.

926 [Richardson, A. D.,](#) Keenan, T. F., Migliavacca, M., Ryu, Y., Sonnentag, O., and Toomey,
927 M.: Climate change, phenology, and phenological control of vegetation feedbacks to
928 the climate system, *Agr Forest Meteorol*, 169, 156-173, 2013.

929 Ruehr, N. K., Martin, J. G., and Law, B. E.: Effects of water availability on carbon and
930 water exchange in a young ponderosa pine forest: Above- and belowground
931 responses, *Agr Forest Meteorol*, 164, 136-148, doi:10.1016/J.Agrformet.2012.05.015,
932 2012.

933 Sarmiento, J. L., Gloor, M., Gruber, N., Beaulieu, C., Jacobson, A. R., Fletcher, S. E. M.,
934 Pacala, S., and Rodgers, K.: Trends and regional distributions of land and ocean
935 carbon sinks, *Biogeosciences*, 7, 2351-2367, doi:10.5194/Bg-7-2351-2010, 2010.

936 Schaefer, K., Collatz, G. J., Tans, P., Denning, A. S., Baker, I., Berry, J., Prihodko, L.,
937 Suits, N., and Philpott, A.: Combined Simple Biosphere/Carnegie-Ames-Stanford
938 Approach terrestrial carbon cycle model, *J. Geophys. Res.*, 113, G03034,
939 doi:10.1029/2007jg000603, 2008.

- 940 Scott, C. E., Rap, A., Spracklen, D. V., Forster, P. M., Carslaw, K. S., Mann, G. W.,
 941 Pringle, K. J., Kivekas, N., Kulmala, M., Lihavainen, H., and Tunved, P.: The direct
 942 and indirect radiative effects of biogenic secondary organic aerosol, *Atmos Chem*
 943 *Phys*, 14, 447-470, doi:10.5194/Acp-14-447-2014, 2014.
- 944 Sindelarova, K., Granier, C., Bouarar, I., Guenther, A., Tilmes, S., Stavrakou, T., Muller,
 945 J. F., Kuhn, U., Stefani, P., and Knorr, W.: Global data set of biogenic VOC
 946 emissions calculated by the MEGAN model over the last 30 years, *Atmos Chem*
 947 *Phys*, 14, 9317-9341, doi:10.5194/Acp-14-9317-2014, 2014.
- 948 Sitch, S., Friedlingstein, P., Gruber, N., Jones, S. D., Murray-Tortarolo, G., Ahlström, A.,
 949 Doney, S. C., Graven, H., Heinze, C., Huntingford, C., Levis, S., Levy, P. E., Lomas,
 950 M., Poulter, B., Viovy, N., Zaehle, S., Zeng, N., Arneth, A., Bonan, G., Bopp, L.,
 951 Canadell, J. G., Chevallier, F., Ciais, P., Ellis, R., Gloor, M., Peylin, P., Piao, S. L.,
 952 Quéré, C. L., Smith, B., Zhu, Z., and Myneni, R.: Recent trends and drivers of
 953 regional sources and sinks of carbon dioxide, *Biogeosciences*, 12, 653-679, 2015.
- 954 Stavrakou, T., Muller, J. F., Bauwens, M., De Smedt, I., Van Roozendael, M., Guenther,
 955 A., Wild, M., and Xia, X.: Isoprene emissions over Asia 1979-2012: impact of
 956 climate and land-use changes, *Atmos Chem Phys*, 14, 4587-4605, doi:10.5194/Acp-
 957 14-4587-2014, 2014.
- 958 Sun, Z. H., Hve, K., Vislap, V., and Niinemets, U.: Elevated [CO₂] magnifies isoprene
 959 emissions under heat and improves thermal resistance in hybrid aspen, *J Exp Bot*, 64,
 960 5509-5523, doi:10.1093/jxb/ert318, 2013.
- 961 Unger, N., Harper, K., Zheng, Y., Kiang, N. Y., Aleinov, I., Arneth, A., Schurgers, G.,
 962 Amelynck, C., Goldstein, A., Guenther, A., Heinesch, B., Hewitt, C. N., Karl, T.,
 963 Laffineur, Q., Langford, B., McKinney, K. A., Misztal, P., Potosnak, M., Rinne, J.,
 964 Pressley, S., Schoon, N., and Serça, D.: Photosynthesis-dependent isoprene emission
 965 from leaf to planet in a global carbon-chemistry-climate model, *Atmos. Chem. Phys.*,
 966 13, 10243-10269, doi:10.5194/acp-13-10243-2013, 2013.
- 967 Unger, N.: On the role of plant volatiles in anthropogenic global climate change,
 968 *Geophys Res Lett*, 41, 8563-8569, doi:10.1002/2014gl061616, 2014.
- 969 Uppala, S. M., Kallberg, P. W., Simmons, A. J., Andrae, U., Bechtold, V. D., Fiorino,
 970 M., Gibson, J. K., Haseler, J., Hernandez, A., Kelly, G. A., Li, X., Onogi, K.,
 971 Saarinen, S., Sokka, N., Allan, R. P., Andersson, E., Arpe, K., Balmaseda, M. A.,
 972 Beljaars, A. C. M., Van De Berg, L., Bidlot, J., Bormann, N., Cairnes, S., Chevallier,
 973 F., Dethof, A., Dragosavac, M., Fisher, M., Fuentes, M., Hagemann, S., Holm, E.,
 974 Hoskins, B. J., Isaksen, I., Janssen, P. A. E. M., Jenne, R., McNally, A. P., Mahfouf,
 975 J. F., Morcrette, J. J., Rayner, N. A., Saunders, R. W., Simon, P., Sterl, A., Trenberth,
 976 K. E., Untch, A., Vasiljevic, D., Viterbo, P., and Woollen, J.: The ERA-40 re-
 977 analysis, *Q J Roy Meteor Soc*, 131, 2961-3012, doi:10.1256/Qj.04.176, 2005.
- 978 von Caemmerer, S., and Farquhar, G. D.: Some Relationships between the Biochemistry
 979 of Photosynthesis and the Gas-Exchange of Leaves, *Planta*, 153, 376-387, 1981.
- 980 Weedon, G. P., Gomes, S., Viterbo, P., Shuttleworth, W. J., Blyth, E., Osterle, H., Adam,
 981 J. C., Bellouin, N., Boucher, O., and Best, M.: Creation of the WATCH Forcing Data
 982 and Its Use to Assess Global and Regional Reference Crop Evaporation over Land
 983 during the Twentieth Century, *J Hydrometeorol*, 12, 823-848,
 984 doi:10.1175/2011jhm1369.1, 2011.

Xu Yue 10/10/15 6:48 PM

Deleted: 17717-17791

986 Weedon, G. P., Balsamo, G., Bellouin, N., Gomes, S., Best, M. J., and Viterbo, P.: The
987 WFDEI meteorological forcing data set: WATCH Forcing Data methodology applied
988 to ERA-Interim reanalysis data, *Water Resources Research*, 50, 7505-7514,
989 doi:10.1002/2014wr015638, 2014.

990 Wofsy, S. C., Goulden, M. L., Munger, J. W., Fan, S. M., Bakwin, P. S., Daube, B. C.,
991 Bassow, S. L., and Bazzaz, F. A.: Net Exchange of Co₂ in a Midlatitude Forest,
992 *Science*, 260, 1314-1317, doi:10.1126/Science.260.5112.1314, 1993.

993 Wu, Z. T., Dijkstra, P., Koch, G. W., Penuelas, J., and Hungate, B. A.: Responses of
994 terrestrial ecosystems to temperature and precipitation change: a meta-analysis of
995 experimental manipulation, *Global Change Biol*, 17, 927-942, doi:10.1111/J.1365-
996 2486.2010.02302.X, 2011.

997 Xia, J. B., Zhang, G. C., Wang, R. R., and Zhang, S. Y.: Effect of soil water availability
998 on photosynthesis in *Ziziphus jujuba* var. *spinosa* in a sand habitat formed from
999 seashells: Comparison of four models, *Photosynthetica*, 52, 253-261, doi:Doi
1000 10.1007/S11099-014-0030-0, 2014.

1001 Yue, X., and Unger, N.: Ozone vegetation damage effects on gross primary productivity
1002 in the United States, *Atmos. Chem. Phys.*, 14, 9137-9153, doi:10.5194/acp-14-9137-
1003 2014, 2014.

1004 Yue, X., and Unger, N.: The Yale Interactive terrestrial Biosphere model: description,
1005 evaluation and implementation into NASA GISS ModelE2, *Geosci. Model Dev.*, 8,
1006 2399-2417, doi:10.5194/gmd-8-2399-2015, 2015.

1007 Yue, X., Unger, N., Keenan, T. F., Zhang, X., and Vogel, C. S.: Probing the past 30-year
1008 phenology trend of U.S. deciduous forests, *Biogeosciences*, 12, 4693-4709,
1009 doi:10.5194/bg-12-4693-2015, 2015.

1010 Zhao, M. S., Heinsch, F. A., Nemani, R. R., and Running, S. W.: Improvements of the
1011 MODIS terrestrial gross and net primary production global data set, *Remote Sens*
1012 *Environ*, 95, 164-176, doi:10.1016/J.Rse.2004.12.011, 2005.

1013 Zhao, M. S., and Running, S. W.: Drought-Induced Reduction in Global Terrestrial Net
1014 Primary Production from 2000 Through 2009, *Science*, 329, 940-943,
1015 doi:10.1126/Science.1192666, 2010.

1016 Zheng, Y., Unger, N., Barley, M., and Yue, X.: Relationships between photosynthesis
1017 and formaldehyde as a probe of isoprene emission, *Atmos. Chem. Phys.*, 15, 8559-
1018 8576, doi:10.5194/acp-15-8559-2015, 2015.

1019 Zhu, Z. C., Bi, J., Pan, Y. Z., Ganguly, S., Anav, A., Xu, L., Samanta, A., Piao, S. L.,
1020 Nemani, R. R., and Myneni, R. B.: Global Data Sets of Vegetation Leaf Area Index
1021 (LAI)_{3g} and Fraction of Photosynthetically Active Radiation (FPAR)_{3g} Derived
1022 from Global Inventory Modeling and Mapping Studies (GIMMS) Normalized
1023 Difference Vegetation Index (NDVI)_{3g} for the Period 1981 to 2011, *Remote Sens*, 5,
1024 927-948, doi:10.3390/Rs5020927, 2013.

1025

1026

Xu Yue 10/10/15 6:48 PM

Deleted: 2014.

1028
1029
1030
1031

Table 1. Summary of model simulations driven with WFDEI reanalysis.

Simulations	Descriptions
CO2_MET_LUC	Annually updated [CO ₂] and land cover, and hourly meteorology. All forcings vary for 1980-2011.
CO2_MET	Annually updated [CO ₂] and hourly meteorology for 1980-2011, land cover is prescribed at the year 1980.
CO2_ONLY	Annually updated [CO ₂] for 1980-2011, land cover is prescribed and hourly meteorology is recycled for the year 1980.
MET_ONLY	Hourly meteorology varies for 1980-2011. [CO ₂] and land cover are prescribed at the year 1980.
LUC_ONLY	Annually updated land cover for 1980-2011, [CO ₂] is prescribed and hourly meteorology is recycled for the year 1980.
TEMP_ONLY	Hourly temperature for 1980-2011 but other meteorological variables are recycled for 1980. [CO ₂] and land cover are prescribed at the year 1980.
PAR_ONLY	Hourly PAR for 1980-2011 but other meteorological variables are recycled for 1980. [CO ₂] and land cover are prescribed at the year 1980.
SOILW_ONLY	Hourly soil wetness for 1980-2011 but other meteorological variables are recycled for 1980. [CO ₂] and land cover are prescribed at the year 1980.
LAI_ONLY	Hourly meteorology is recycled for the year 1980. [CO ₂] and land cover are prescribed at the year 1980. Leaf area index varies for 1980-2011.
PHEN_ONLY	Hourly meteorology is recycled for the year 1980. [CO ₂] and land cover are prescribed at the year 1980. Phenology varies for 1980-2011.

1032
1033
1034
1035
1036
1037

1038
 1039
 1040
 1041
 1042
 1043
 1044

Table 2. Summary of trends in different domains from the simulation CO2_MET_LUC, which is driven with WFDEI meteorology. Significant trends ($p < 0.05$) are indicated with asterisks.

Regions	Amazon	North America	Central Africa	Europe	East Asia	Indonesia
LAI ($10^{-3} \text{ m}^2 \text{ m}^{-2} \text{ a}^{-1}$)	0.8	0.4 *	1.8 *	3.5 *	-0.4 *	-0.1
GPP (Tg C a^{-2})	52.7 *	13.6	83.3 *	53.4 *	42.4 *	15.3 *
NPP (Tg C a^{-2})	27.1 *	9.7	51.7 *	33.2 *	27.2 *	11.4 *
NEP (Tg C a^{-2})	-8.1	-1.7	11.6	6.7	-6.2	0.2
Ra (Tg C a^{-2})	25.6 *	3.9	31.6 *	20.2 *	15.2 *	3.9 *
Rh (Tg C a^{-2})	35.2 *	11.2 *	39.8 *	26.6 *	33.4 *	11.2 *
Isoprene PS_BVOC (Tg C a^{-2})	0.04	-0.03	0.25 *	0.16 *	-0.02	-0.01
Isoprene MEGAN (Tg C a^{-2})	-0.43 *	-0.07 *	-0.14 *	0.10 *	-0.13 *	-0.16 *
Monoterpene (Tg C a^{-2})	-0.03 *	0.01	-0.002	0.03 *	-0.02 *	-0.02 *
Budburst (days a^{-1})	N/A ^a	-0.01	N/A	-0.16 *	-0.15 *	N/A
Dormancy onset (days a^{-1})	N/A	0.09 *	N/A	0.16 *	0.03	N/A
Season extension (days a^{-1})	N/A	0.1 *	N/A	0.32 *	0.18 *	N/A

1045
 1046
 1047

^a Phenology is set to constant for tropical rainforest in the model.

1048
1049
1050
1051
1052
1053
1054

Table 3. Summary of simulated trends of global carbon fluxes (Tg C a⁻²) from different experiments. Simulations are using WFDEI meteorology. Significant trends ($p < 0.05$) are indicated with asterisks.

Simulations	GPP	NPP	NEP	Ra	Rh
CO2_MET_LUC	297.4 *	185.3 *	2.7	112.1 *	180.9 *
CO2_MET	329.5 *	206.2 *	4.5	123.3 *	199.8 *
CO2_ONLY	412.4 *	299 *	66.2 *	113.5 *	231.9 *
MET_ONLY	-108.6 *	-108.2 *	-72.6 *	-0.4	-35
LUC_ONLY	-13 *	-8 *	-34.6 *	-5 *	26.9 *
TEMP_ONLY	-23.2 *	-56 *	-10.2 *	32.8 *	-43.6 *
PAR_ONLY	-5.9	-5.8	-23.4 *	-0.1	18.3 *
SOILW_ONLY	-84.8 *	-51 *	-13.1 *	-33.8 *	-38.3
LAI_ONLY	-8.8	-25.6 *	-44.5 *	16.7 *	18.7 *
PHEN_ONLY	-103.1 *	-56.2 *	47.1 *	-46.8 *	-102.9 *

1055
1056

1057 **Figure Captions**

1058

1059 **Figure 1.** Comparison of trends in (b-f) simulated leaf area index (LAI) with (a)
1060 observations for 1982-2011. Observations are derived from GIMMS NDVI. Simulations
1061 are performed with either (d, e, f) single forcings or (b, c) the combinations of these
1062 forcings. Forcings considered include meteorology from WFDEI reanalysis (MET), CO₂
1063 fertilization (CO₂), and land use change (LUC). For every forcing included in the
1064 simulation, the year-to-year fields are utilized. Otherwise, the forcing is prescribed at the
1065 year 1980. Only significant trends ($p < 0.05$) are presented. The six box regions in (a)
1066 indicate areas for statistical analyses in Table 2.

1067

1068 **Figure 2.** Simulated trends in (a) gross primary productivity (GPP), (c) net primary
1069 productivity (NPP), and (e) net ecosystem productivity (NEP), and (b, d, f) the dominant
1070 drivers for these changes during 1982-2011. Simulations are performed with WFDEI
1071 reanalysis. Three factors, meteorological forcing, CO₂ fertilization, and land use change,
1072 are considered as the potential drivers of flux trends. For each grid in figures (b, d, f), the
1073 factor generating the largest (either maximum or minimum) trend with the same sign as
1074 the net change (a, c, e) is selected as the driving factor. Only significant trends ($p < 0.05$)
1075 are presented.

1076

1077 **Figure 3.** Comparisons of trends in (a, b) GPP and (c, d) NPP for 2000-2011 between (a,
1078 c) simulations and (b, d) observations. Observed fluxes are retrieved from the Moderate
1079 Resolution Imaging Spectroradiometer (MODIS).

1080

1081 **Figure 4.** Simulated (a) trends in GPP driven alone with WFDEI reanalysis and the (b)
1082 drivers for such changes. Simulation in (a) is performed with year-to-year meteorological
1083 forcings but prescribed [CO₂] and land use in the year 1980. Simulations in (b) are the
1084 same as (a) except that the year-to-year variations are allowed only for a single
1085 meteorological variable (temperature, PAR, or soil wetness) each time. For each grid, the
1086 meteorological variable generating the largest (either maximum or minimum) trend with

1087 the same sign as the net change (a) is selected as the driving factor. Only significant
1088 trends ($p < 0.05$) are presented.

1089

1090 **Figure 5.** Global total fluxes of GPP, NPP, Rh (heterotrophic respiration), and NEP from
1091 different sensitivity simulations with all forcings (black), meteorology alone (red), CO₂
1092 alone (green), and land use change alone (blue).

1093

1094 **Figure 6.** Simulated trends of (a, c) isoprene and (e) monoterpene, and (b, d, f) the
1095 dominant drivers for these changes during 1982-2011. Simulations are performed with
1096 WFDEI reanalysis. Isoprene emissions are simulated with (a) PS_BVOC and (c)
1097 MEGAN schemes. Three factors, meteorological forcing, CO₂ effects (both fertilization
1098 and inhibition), and land use change, are considered as the potential drivers of flux
1099 trends. For each grid in figures (b, d, f), the factor generating the largest (either maximum
1100 or minimum) trend with the same sign as the net change (a-c) is selected as the driving
1101 factor. Only significant trends ($p < 0.05$) are presented.

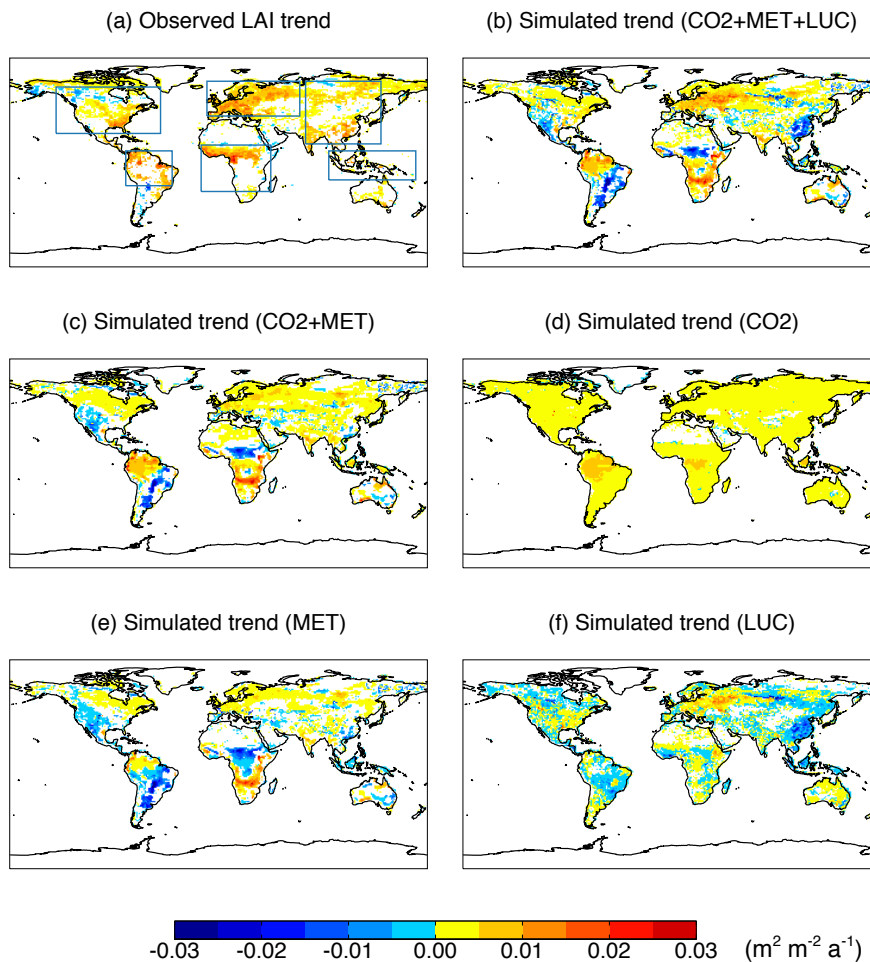
1102

1103 **Figure 7.** Responses of (a) GPP and (b) isoprene emissions to the changes in the annual
1104 average LAI at the north of 30°N for simulations CO₂_MET (red) and LAI_ONLY
1105 (blue). Both GPP and isoprene emissions are the sum of all PFTs. Isoprene is simulated
1106 with the PS_BVOC scheme. Units of trends are (a) Pg C a⁻¹ LAI⁻¹ and (b) Tg C a⁻¹ LAI⁻¹.
1107 The spatial distribution of GPP and isoprene changes is shown in Figure S2.

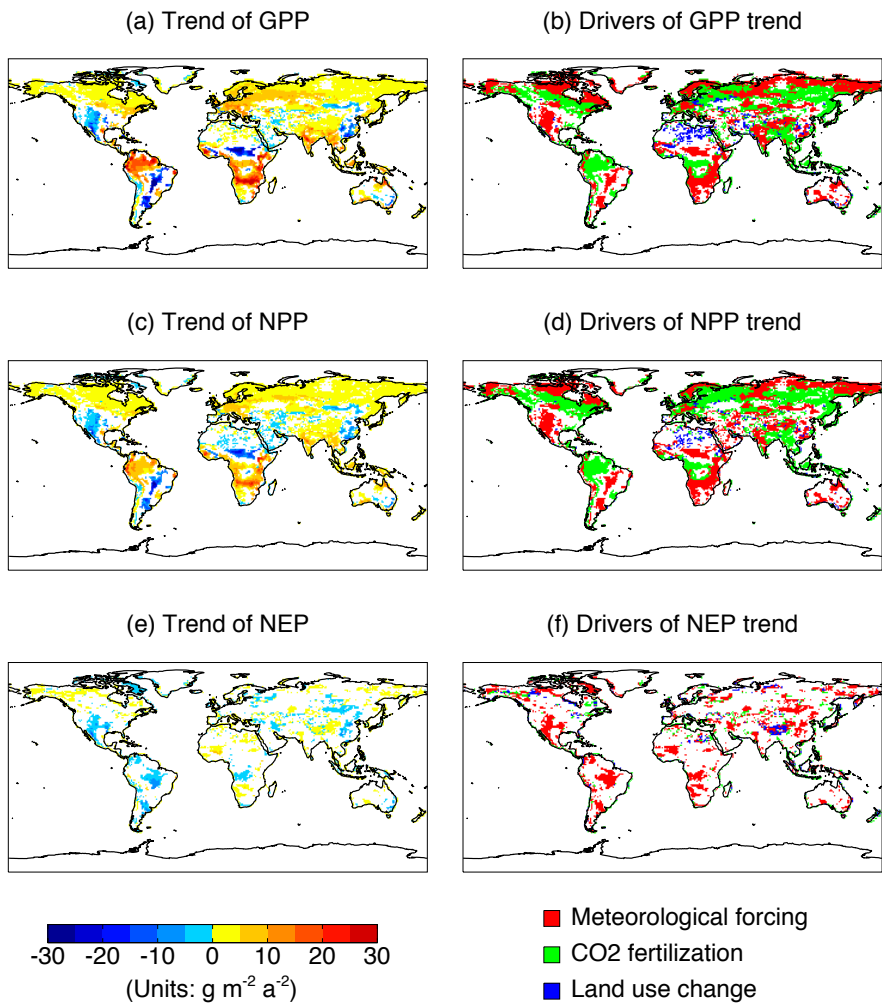
1108

1109 **Figure 8.** Predicted trend in (a) budburst and (b) dormancy onset dates over north of
1110 30°N and the responses of (c) GPP and (d) isoprene emissions to the changes in the
1111 growing length. Both GPP and isoprene emissions are the sum of DBF, shrub, grassland,
1112 and tundra. Isoprene is simulated with the PS_BVOC scheme. For the bottom panel,
1113 different colors indicate sensitivity experiments with different year-to-year forcings: CO₂
1114 and meteorology (red), temperature only (magenta), and phenology only (blue). Units of
1115 trends are (a) day a⁻¹, (b) day a⁻¹, (c) Pg C a⁻¹ day⁻¹, and (d) Tg C a⁻¹ day⁻¹. The spatial
1116 distribution of GPP and isoprene changes is shown in Figure S2.

1117

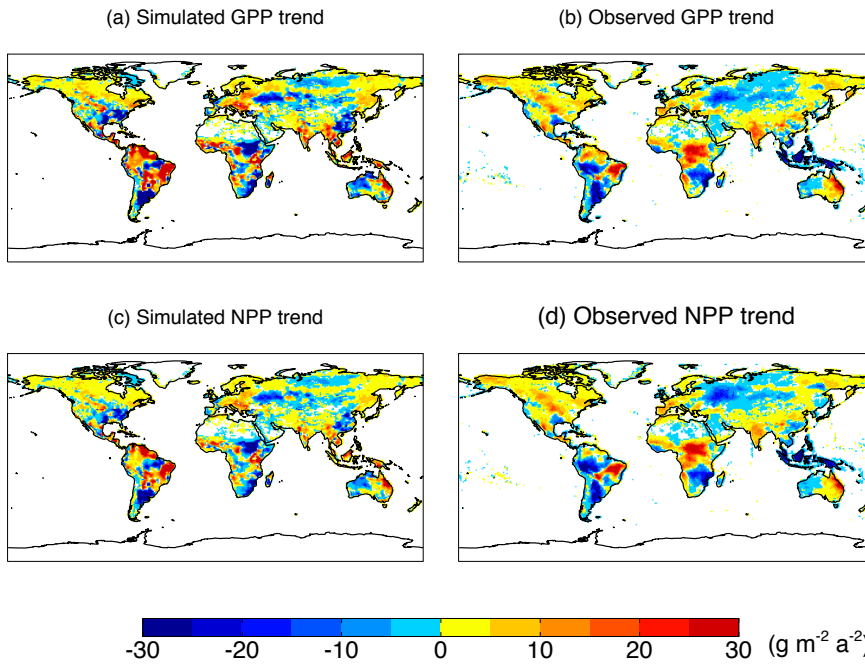


1118
 1119 **Figure 1.** Comparison of trends in (b-f) simulated leaf area index (LAI) with (a)
 1120 observations for 1982-2011. Observations are derived from GIMMS NDVI. Simulations
 1121 are performed with either (d, e, f) single forcings or (b, c) the combinations of these
 1122 forcings. Forcings considered include meteorology from WFDEI reanalysis (MET), CO₂
 1123 fertilization (CO₂), and land use change (LUC). For every forcing included in the
 1124 simulation, the year-to-year fields are utilized. Otherwise, the forcing is prescribed at the
 1125 year 1980. Only significant trends ($p < 0.05$) are presented. The six box regions in (a)
 1126 indicate areas for statistical analyses in Table 2.
 1127
 1128
 1129



1130
 1131 **Figure 2.** Simulated trends in (a) gross primary productivity (GPP), (c) net primary
 1132 productivity (NPP), and (e) net ecosystem productivity (NEP), and (b, d, f) the dominant
 1133 drivers for these changes during 1982-2011. Simulations are performed with WFDEI
 1134 reanalysis. Three factors, meteorological forcing, CO₂ fertilization, and land use change,
 1135 are considered as the potential drivers of flux trends. For each grid in figures (b, d, f), the
 1136 factor generating the largest (either maximum or minimum) trend with the same sign as
 1137 the net change (a, c, e) is selected as the driving factor. Only significant trends ($p < 0.05$)
 1138 are presented.
 1139
 1140

1141
1142



1143
1144 **Figure 3.** Comparisons of trends in (a, b) GPP and (c, d) NPP for 2000-2011 between (a,
1145 c) simulations and (b, d) observations. Observed fluxes are retrieved from the Moderate
1146 Resolution Imaging Spectroradiometer (MODIS).

1147
1148
1149
1150
1151
1152
1153

1154
1155
1156
1157
1158
1159
1160
1161
1162
1163
1164
1165
1166
1167
1168
1169
1170
1171
1172
1173
1174
1175
1176
1177
1178
1179
1180
1181
1182
1183
1184
1185
1186
1187
1188
1189
1190
1191
1192

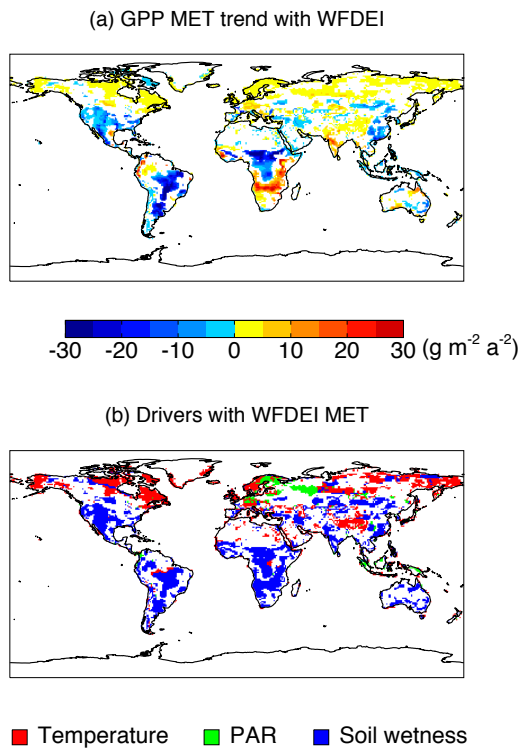
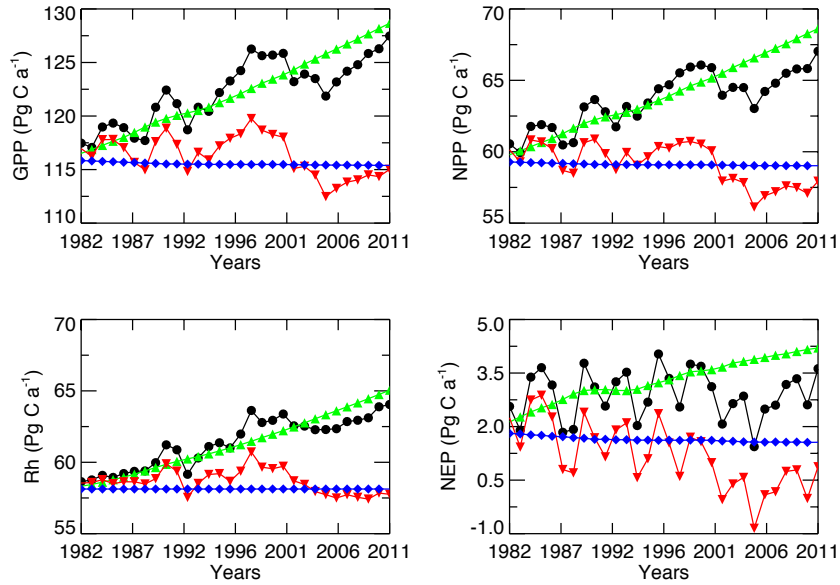
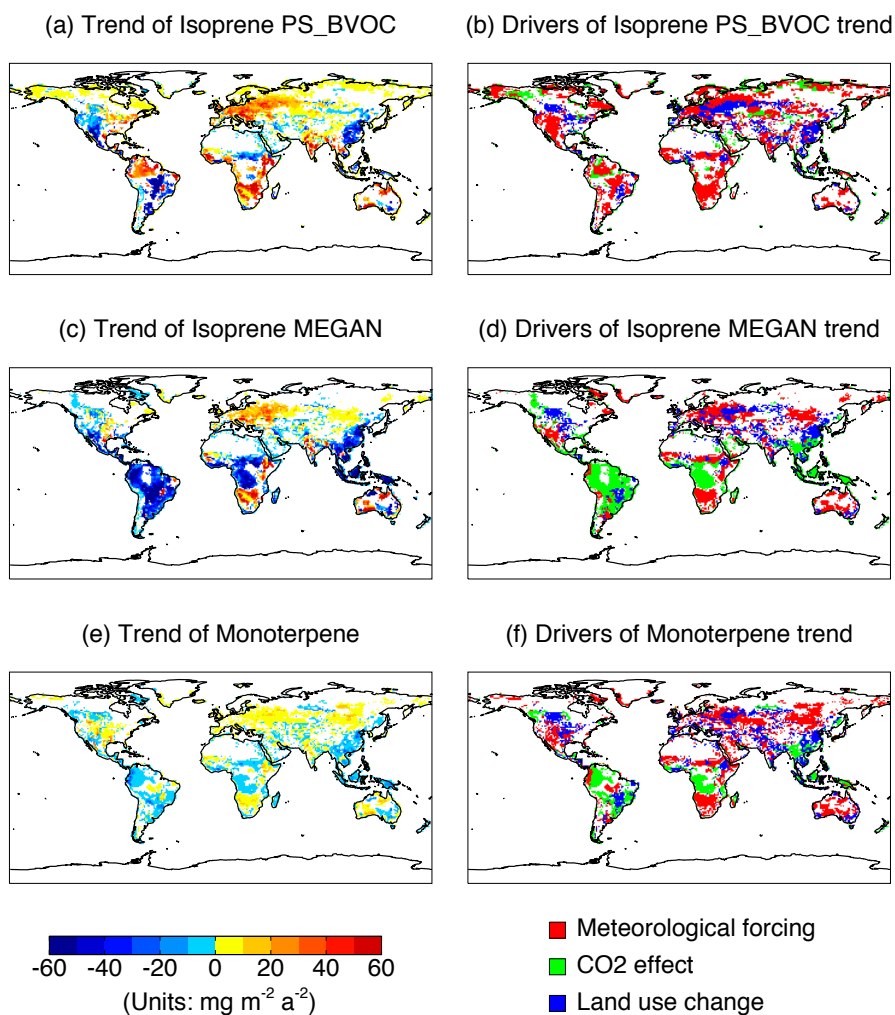


Figure 4. Simulated (a) trends in GPP driven alone with WFDEI reanalysis and the (b) drivers for such changes. Simulation in (a) is performed with year-to-year meteorological forcings but prescribed $[\text{CO}_2]$ and land use in the year 1980. Simulations in (b) are the same as (a) except that the year-to-year variations are allowed only for a single meteorological variable (temperature, PAR, or soil wetness) each time. For each grid, the meteorological variable generating the largest (either maximum or minimum) trend with the same sign as the net change (a) is selected as the driving factor. Only significant trends ($p < 0.05$) are presented.

1193
1194
1195
1196
1197
1198



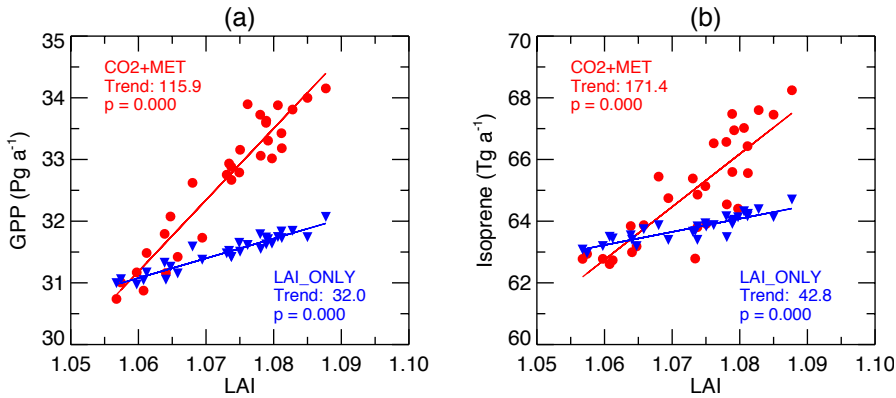
1199 **Figure 5.** Global total fluxes of GPP, NPP, Rh (heterotrophic respiration), and NEP from
1200 different sensitivity simulations with all forcings (black), meteorology only (red), CO₂
1201 alone (green), and land use change alone (blue).
1202



1203
 1204
 1205
 1206
 1207
 1208
 1209
 1210
 1211
 1212

Figure 6. Simulated trends of (a, c) isoprene and (e) monoterpene, and (b, d, f) the dominant drivers for these changes during 1982-2011. Simulations are performed with WFDEI reanalysis. Isoprene emissions are simulated with (a) PS_BVOC and (c) MEGAN schemes. Three factors, meteorological forcing, CO₂ effects (both fertilization and inhibition), and land use change, are considered as the potential drivers of flux trends. For each grid in figures (b, d, f), the factor generating the largest (either maximum or minimum) trend with the same sign as the net change (a-c) is selected as the driving factor. Only significant trends ($p < 0.05$) are presented.

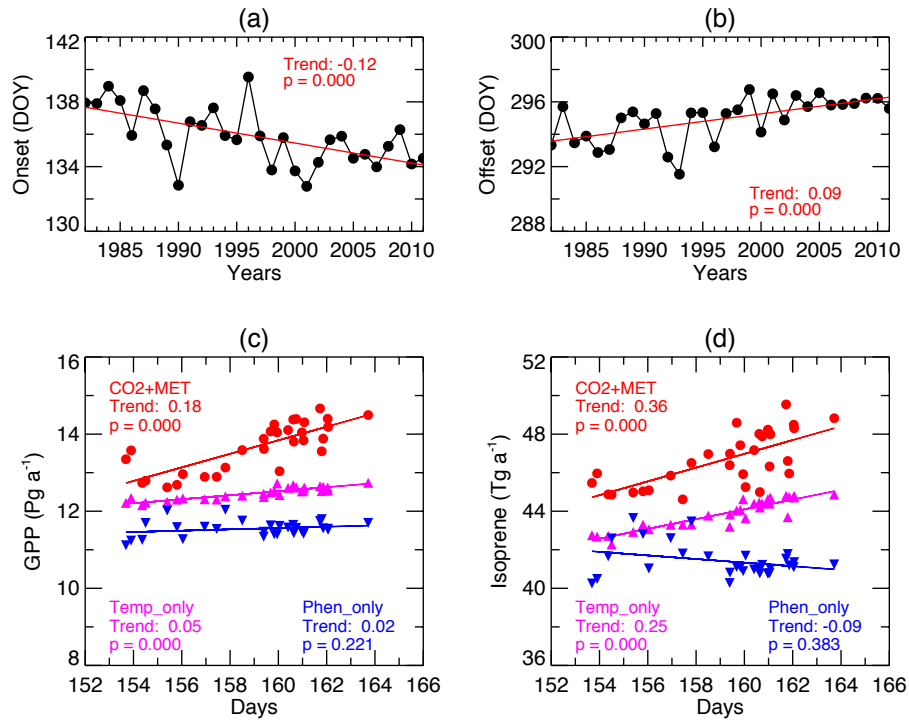
1213
1214
1215
1216
1217



1218
1219
1220
1221
1222
1223
1224
1225

Figure 7. Responses of (a) GPP and (b) isoprene emissions to the changes in the annual average LAI at the north of 30°N for simulations CO2_MET (red) and LAI_ONLY (blue). Both GPP and isoprene emissions are the sum of all PFTs. Isoprene is simulated with the PS_BVOC scheme. Units of trends are (a) Pg C a⁻¹ LAI⁻¹ and (b) Tg C a⁻¹ LAI⁻¹. The spatial distribution of GPP and isoprene changes is shown in Figure S2.

1226
1227



1228

1229 **Figure 8.** Predicted trend in (a) budburst and (b) dormancy onset dates over north of
1230 30°N and the responses of (c) GPP and (d) isoprene emissions to the changes in the
1231 growing length. Both GPP and isoprene emissions are the sum of DBF, shrub, grassland,
1232 and tundra. Isoprene is simulated with the PS_BVOC scheme. For the bottom panel,
1233 different colors indicate sensitivity experiments with different year-to-year forcings: CO₂
1234 and meteorology (red), temperature only (magenta), and phenology only (blue). Units of
1235 trends are (a) day a⁻¹, (b) day a⁻¹, (c) Pg C a⁻¹ day⁻¹, and (d) Tg C a⁻¹ day⁻¹. The spatial
1236 distribution of GPP and isoprene changes is shown in Figure S2.

1237

1238

1239